UC San Diego

UC San Diego Electronic Theses and Dissertations

Title

Functionalization of nanocarriers for efficient combination drug delivery

Permalink

https://escholarship.org/uc/item/0gs5c83k

Author

Hu, Che-Ming Jack

Publication Date

2011

Peer reviewed|Thesis/dissertation

eScholarship.org Powered by the California Digital Library
University of California

UNIVERSITY OF CALIFORNIA, SAN DIEGO

Functionalization of Nanocarriers for Efficient Combination Drug Delivery

A dissertation submitted in partial satisfaction of the requirements for the degree
Doctor of Philosophy

in

Bioengineering

by

Che-Ming Jack Hu

Committee in charge:

Professor Michael J. Heller, Chair
Professor Liangfang Zhang, Co-Chair
Professor Sadik C. Esener
Professor Shyni Varghese
Professor Joseph Wang

2011

©
Che-Ming Jack Hu, 2011
All rights reserved

The Dissertation of Che-Ming Jack Hu is approved, and it is acceptable in quality and form for publication on microfilm and electronically:

_____

_____

_____

_____
Co-Chair

_____
Chair

University of California, San Diego

2011

DEDICATION

This dissertation is dedicated to my loving parents, Mao-Tso Hu and Yu-Hsia Hu, who have made countless sacrifices so I could freely pursue my dreams.

EPIGRAPH

"Imagination is more important than knowledge. Knowledge is limited. Imagination encircles the world."

Albert Einstein

TABLE OF CONTENTS

Signature page……iii

Dedication……...iv

Epigraph……...v

Table of Contents……....vi

List of Figures……ix

List of Tables. ……...xii

Acknowledgements……..xiii

Vita……... .xv

Abstract of the Dissertation…….xvii

Chapter 1 Introduction……... 1
1.1 Barriers in Cancer Drug Delivery……..1
1.2 Nanoparticles for Effective Cancer Drug Delivery……...5
1.2.1 Prolonged Drug Systemic Circulation Lifetime……5
1.2.2 Targeted Drug Delivery……..8
1.2.3 Endocytic Uptake of Drugs……...10
1.2.4 Co-delivery of Multiple Therapeutic Agents in Combination…..12
1.3 Challenges in Nanoparticle Drug Delivery…… 17
1.3.1 Challenges in Multi-drug Coencapsulation in Nanoparticles…...17
1.3.2 Challenges in Tumor-targeted Nanoparticles……...18
1.3.3 Challenges in Long-circulating Nanoparticles……18

Chapter 2 Polymeric Nanoparticles with Precise
Ratiometric Control over Drug Loading……... 20

2.1 Introduction……20
2.2 Experimental Methods……23
2.2.1 Materials……...23
2.2.2 Synthesis of 2-((2,6-diisopropylphenyl)amino)-4-((2,6-diisopropylphenyl)imino)-2-pentene (BDI)……24
2.2.3 Synthesis of (BDI)ZnN($SiMe_3$)$_2$ Catalyst……25
2.2.4 Ring Opening Polymerization of l-lactide……26

2.2.5 Preparation of Lipid-Coated Drug-Polymer Nanoparticles……26
2.2.6 Cellular Colocalization and Cytotoxicity Studies……28
2.3 Results and Discussion……29
2.3.1 Synthesis and Characterization of Drug-Polymer Conjugates….29
2.3.2 Synthesis and Characterization of Dual-Drug Loaded Polymeric Nanoparticles……31
2.3.3 Ratiometric Control over Dual-Drug Loading ……32
2.3.4 Dual-Drug Colocalization and Cellular Internalization……..…. 34
2.3.5 *In vitro* Cytotoxicity of Dual-Drug Nanoparticles ……... 36
2.4 Conclusion……...38

Chapter 3 Half-antibody Functionalized Nanoparticles for Targeted Drug Delivery……40
3.1 Introduction……40
3.2 Experimental Methods……43
3.2.1 Conjugation of Fluorophore to Anti-CEA Antibody and PLGA Polymer……... 43
3.2.2 Synthesis and Characterization of Anti-CEA hAb Targeted Lipid-polymer Hybrid NPs……44
3.2.3 Cellular Targeting and Internationalization Studies……46
3.2.4 *In vitro* Cytotoxicity Study……...47
3.3 Results and Discussion……49
3.3.1 Synthesis of Anti-CEA hAb……50
3.3.2 Synthesis and Characterization of hAb-NP conjugates……52
3.3.3 Targeting Ability of hAb NPs……... 54
3.3.4 Cytotoxicity of Paclitaxel-loaded hAb-NPs……56
3.4 Conclusion……...59

Chapter 4 Erythrocyte Membrane-camouflaged Polymeric Nanoparticles as a Novel Long-circulating Delivery Platform……..... 60
4.1 Introduction……60
4.2 Experimental Methods……62
4.2.1 Red Blood Cell Ghost Derivation……62
4.2.2 Preparation of RBC Membrane-derived Vesicles……63
4.2.3 Preparation of PLGA Nanoparticles……64
4.2.4 Fusion of RBC Membrane-derived Vesicles with PLGA Nanoparticles……65
4.2.5 Characterization of RBC Membrane-coated PLGA Nanoparticles……66
4.2.6 Transmission Electron Microscopy Imaging……66
4.2.7 Tissue Culture and Nanoparticle Endocytosis……..67
4.2.8 Protein Characterization Using SDS PAGE……68

4.2.9 Pharmacokinetics and Biodistribution Study……... 68
4.3 Results and Discussion……69
4.3.1 Preparation of RBC Membrane Coated NPs……69
4.3.2 Characterization of RBC Membrane Coated NPs……72
4.3.3 Stability and Circulation Half-life of RBC Membrane Coated NPs……... 76
4.3.4 Biodistributions of RBC Membrane Coated NPs……..80
4.4 Conclusion……...84

Chapter 5 Conclusions and Future Directions…… 85
5.1 PLGA Vaccine Delivery Vehicles…….. 86
5.2 PEG Shedding Drug Delivery Vehicle……87
5.3 Biomimetic Stabilizer to Replace PEG……... 89

References……90

LIST OF FIGURES

Fig. 1.1…..……..4
Schematic illustration of nanoscale drug carriers (a) liposome, (b) polymeric micelle, (c) polymer-drug conjugate, (d) dendrimer, (e) oil nanoemulsion, (f) mesoporous silica nanoparticle, and (g) iron oxide nanoparticle.

Fig. 1.2……..……..6
Schematic illustration of the enhanced permeation and retention (EPR) effect in solid tumors. Leaky vasculature and poor lymphatic drainage cause enhanced permeation and retention of nanoscale particles. Nanoparticles that are long-circulating can maximize tumoral uptake through EPR effect.

Fig. 1.3……..……11
Schematic illustration of NP endocytosis to cross the membrane barrier for cellular entry.

Fig. 1.4……..……14
Schematic presentation of combinatorial nanoparticles containing chemosensitizers and chemotherapeutics against MDR of a cancer cell.

Fig. 2.1……..……23
Schematic illustration of a dual-drug loaded lipid-polymer hybrid nanoparticle, of which the polymeric core consists of two distinct drug-polymer conjugates with ratiometric control over drug loading.

Fig. 2.2……..……30
Chemical characterization of the drug-polymer conjugates. (A) Schematic description of the living ring-opening polymerization of l-lactide catalyzed by an activated metal alkoxide complex. (B) Qualitative ^{1}H-NMR spectra showing the characteristic proton resonance peaks of DOX-PLA (upper panel) and CPT-PLA (lower panel)...

Fig. 2.3……..……32
Scanning electron microscopy (SEM) and dynamic light scattering (DLS) measurements showing the morphology and size of lipid-polymer hybrid nanoparticles with the polymer cores consisting of: (A) DOX-PLA conjugates, (B) CPT-PLA conjugates, and (C) DOX-PLA and CPT-PLA conjugates with a molar ratio of 1:1

Fig. 2.4……..……33
Quantification of DOX and CPT loading efficiency in dual-drug loaded nanoparticles (containing both DOX-PLA and CAP-PLA) and single-drug loaded nanoparticles (containing DOX-PLA or CPT-PLA), respectively. NPs: nanoparticles.

Fig. 2.5……..……35
Cellular colocalization studies of the DOX-PLA and CPT-PLA loaded dual-drug nanoparticles. Fluorescence microscopy images showing the colocalization of DOX and CPT in the cellular compartment of MDA-MB-435 breast cancer cells.

Fig. 2.6……..……37
A comparative study of cellular cytotoxicity of the DOX-PLA and CPT-PLA loaded dual-drug nanoparticles against the MDA-MB-435 breast cancer cells. The ratios shown in figure legends are the molar ratios of DOX-PLA to CPT-PLA. Solid lines represent the dual-drug loaded nanoparticles and dashed lines represent the cocktail mixture of DOX-PLA loaded and CPT-PLA loaded...

Fig. 3.1....……..……..……..…43
Schematic illustration of hAb functionalized NPs targeting tumor cells through surface antigens.

Fig. 3.2……..……49
Schematic diagram of the synthesis of anti-CEA half-antibody (hAb) conjugated lipid-polymer hybrid NPs.

Fig. 3.3……..……51
(A) Gel electrophoresis results of anti-CEA antibody reduction at TCEP (reducing agent) concentration of 0x, 3x, 10x and 30x over the concentration of the antibody, respectively. The rightmost lane represents a standard molecular weight ladder. (B) Quantifying the conjugation yield of 1 mg...

Fig. 3.4……..……53
(A) Size and surface zeta potential of the hybrid NPs before and after hAb conjugation determined by dynamic light scattering. (B) SEM image of hAb targeted lipid-polymer hybrid NPs.

Fig. 3.5……..……55
Scanning fluorescence microscopy images demonstrated the co-delivery of (A) the lipid shell to which the hAb conjugated (visualized with green Alexa Fluor 488 dyes) and (B) the PLGA polymeric core (visualized with red Alexa Fluor 647 dyes) to CEA-positive BxPC-3 cells (nucleus stained in blue with DAPI)...

Fig. 3.6……..……58
Relative viability of BxPC-3 cells incubated paclitaxel-loaded hAb targeted NPs (solid line) and non-targeted NPs (dashed line) with various paclitaxel loading yields using ATP assay. The results were normalized to controls without NP treatment. ANOVA test: *$p<0.01$ ($n=8$). Inset: paclitaxel loading...

Fig. 4.1…….…….62
Schematic illustration of RBC membrane camouflaged PLGA NPs.

Fig. 4.2……..…….…….…..70
Schematics of the preparation process of the RBC membrane-coated PLGA nanoparticles (NPs)..

Fig. 4.3……...……...70
Phase contrast microscopy images of mouse red blood cells (RBCs) before (left panel) and after (right panel) hemolytic treatment in hypotonic solution. Deprivation of RBC interior contents (hemoglobins) was verified by the change in phase contrast, which indicates an alteration of the medium inside the RBCs.

Fig. 4.4……..…..……...72
The average diameter of the RBC membrane-derived vesicles following RBC ghosts derivation, 5 min of sonication, 400 nm extrusion, and 100 nm extrusion as measured by DLS.

Fig. 4.5……...……...74
Structural characterization of the RBC membrane-coated PLGA nanoparticles. (A) The nanoparticles were negatively stained with uranyl acetate and subsequently visualized with TEM. (B) DLS measurements of the size, polydispersity index (PDI), and surface zeta potential of the nanoparticles over 14 days...

Fig. 4.6……...……...79
Membrane protein retention, particle stability in serum, and the *in vivo* circulation time of the RBC membrane-coated nanoparticles (NPs). (A) Proteins in emptied RBCs, RBC membrane-derived vesicles, and purified RBC membrane-coated PLGA nanoparticles were solubilized and resolved on a...

Fig. 4.7……..…...82
Biodistributions of the RBC membrane-coated polymeric nanoparticles. Fluorescently labeled nanoparticles were injected intravenously into the mice. At each time points (24, 48, and 72 hour respectively), the organs from a randomly grouped subset of mice were collected, homogenized and.

LIST OF TABLES

Table 1.1……...……...…….16
Selected examples of combinatorial nanoparticle formulations containing chemotherapeutics and chemosensitizers.

Table 2.1……...……...…….34
Characteristic features of the lipid-coated drug-polymer conjugate nanoparticles.

ACKNOWLEDGEMENT

I would like to thank Professor Liangfang Zhang first and foremost because this dissertation would not be possible without him. He is an inspirational mentor who has given me knowledge, meaning, and purpose. He showed me all the characters in a great scientist and I am truly blessed to have worked under his guidance.

Professor Michael Heller advised me during the early years of my graduate program. He always made himself available for me, and his colorful personality and anecdotal stories added new perspectives to the way I think.

My colleagues in the Zhang Lab have all made invaluable contributions to my work. Dr. Santosh Aryal is the chemistry wizard behind many of the polymer chemistry schemes for drug encapsulation. Dr. Li Zhang did much of the *in vivo* studies for the RBC membrane coated nanoparticles. Ronnie Fang's specialty in large-scale preparation of nanoparticles has elevated the RBC membrane coated nanoparticles to a different level and working with him made everything so much easier. Jonathan Copp provided much medical insights and helped pushed the RBC nanoparticle platform forward. Dissaya Nu Pornpattananangkul contributed to many discussions and her constant smile, along with the presence of Soracha Kun Thamphiwatana, and Victoria Fu added joy to my graduate experience. I thank Dr. Corbin Clawson and Dr. Marta Sartor who paved the way in the study of nanoparticle drug delivery. And thanks to the undergraduate students, Connie Cheung, Cody Carpenter, and Diana Dehaini for putting up with my peculiar teaching style.

I would like to thank the Siebel Foundation for their generous scholarship that aided me in the last year of my study.

Lastly, I would like to thank the Bioengineering department at UCSD, its faculty and administration staff, for giving me the most memorial, inspiring, and illuminating time of my life.

Chapter 1 is based, in part, on the material as it appears in Current Drug Metabolism, 2009, Che-Ming Hu and Liangfang Zhang, and, in part, on the material submitted for publication as it may appear in Biochemical Pharmacology 2011, Che-Ming Hu and Liangfang Zhang. The dissertation author was the primary investigator and co-author of these papers.

Chapter 2, in full, is a reprint of the material as it appears in Molecular Pharmaceutics, 2011, Che-Ming Hu, Santosh Aryal, and Liangfang Zhang. The dissertation author was the primary investigator and co-author of this paper.

Chapter 3, in full, is a reprint of the material as it appears in Molecular Pharmaceutics, 2010, Che-Ming Hu, Sharmeela Kaushal, Hop S. Tran Cao, Santosh Aryal, Marta Sartor, Sadik Esener, Michael Bouvet, and Liangfang Zhang. The dissertation author was the primary investigator and author of this paper.

Chapter 4, in full, is a reprint of the material as it appears in Proceedings of the National Academy of Sciences, 2011, Che-Ming Hu, Li Zhang, Santosh Aryal, Connie Cheung, Ronnie H. Fang, and Liangfang Zhang. The dissertation author was the primary investigator and author of this paper.

VITA

2005	Bachelor of Science, University of California, Berkeley
2008	Master of Science, University of California, San Diego
2011	Doctor of Philosophy, University of California, San Diego

PUBLICATIONS

1. Hu, C-M.; Zhang, L.; Aryal, S.; Cheung, C.; Fang, R.; Zhang, L. "Erythrocyte membrane-camouflaged polymeric nanoparticles as a biomimetic delivery platform" *Proceedings of the National Academy of Sciences* 2011, 108, 10980-10985.

2. Aryal, S.; Hu, C-M.; Zhang, L. "Polymeric nanoparticles with precise ratiometric control over drug loading for combination therapy" 2011, *Molecular Pharmaceutics* 2011, 8(4), 1401-1407.

3. Balasubramanian, S.; Kagan, D.; Hu, C-M.; Campuzano, S.; Lobo-Castañon, M. ; Lim, N.; Kang, D.; Zhang, L.; Wang, J. "Micromachine enabled selection and isolation of cancer cells in complex media", Angewandte Chemie International Edition 2011, 50, 4161-4164.

4. Hu, C-M.; Kaushal, S; Cao, H. S.; Aryal, S.; Sartor, M.; Esener, S.; Bouvet, M.; Zhang, L. "Half-antibody functionalized lipid-polymer hybrid nanoparticles for targeted drug delivery to carcinoembryonic antigen (CEA) presenting pancreatic cancer cells" *Molecular Pharmaceutics* 2010, 7, 914-920.

5. Fang, R.; Aryal, S.; Hu, C-M.; Zhang, L. "Quick synthesis of lipid-polymer hybrid nanoparticles with low polydispersity using a single-step sonication method", *Langmuir* 2010, *26*, 16958-16962.

6. Aryal, S.; Hu, C-M.; Zhang, L. "Polymer-cisplatin conjugate nanoparticles for acid-responsive drug delivery" *ACS Nano* 2011, 4, 251-258.

7. Hu, C-M.; Aryal, S.; Zhang, L. "Nanoparticles assisted combination therapies for effective cancer treatment", Therapeutic Delivery 2010, 1, 323-334.

8. Zhang, L.; Pornpattananangkul, D.; Hu, C-M.; Huang, C-M. "Development of nanoparticles for antimicrobial drug delivery", *Current Medicinal Chemistry* 2010, *17*, 585-594.

9. Aryal, S.; Hu, C-M.; Zhang, L. "Combinatorial drug conjugation enabled nanoparticle dual drug delivery", *Small* 2010 2010, 6, 1442-1448.

10. Hu, C-M.; Zhang, L. "Therapeutic nanoparticles to combat cancer drug resistance", *Current Drug Metabolism* 2009, 10, 836-841.

11. Lefkowitz, R. B.; Marciniak, J. Y.; Hu, C-M.; Schmid-Schönbein, G.W.; Heller, M. J. "An electrophoretic method for the detection of chymotrypsin and trypsin activity directly in whole blood" *Electrophoresis* 2009*, 31*, 403-410.

12. Stoeber, B.; Hu C-M,; Liepmann D.; Muller, S. J. "Passive flow control in microdevices using thermally responsive polymer solutions", *Physics of Fluids* 2006, 18, 053103.

13. Aryal, S.; Hu, C-M.; Zhang, L. "Nanoparticle drug delivery enhances the toxicity of hydrophobic-hydrophilic drug conjugates" 2011, *Journal of Materials Chemistry* (in press)

14. Hu, C-M.; Zhang, L. "Nanoparticle-based combination therapy to overcome drug resistance in cancer" invited review article to *Biochemical Pharmacology* (manuscript submitted).

15. Aryal, S.; Hu, C-M.; Zhang, L. "Synthesis and Characterization of Ptsome: A Novel Platinum-Based Liposome-Like Nanostructure" *Journal of the American Chemical Society* (manuscript submitted).

FIELDS OF STUDY

Major Field: Drug delivery and Nanoengineering

Studies in Drug delivery and Nanoengineering
Professor Liangfang Zhang

ABSTRACT OF THE DISSERTATION

Functionalization of Nanocarriers for Efficient Combination Drug Delivery

by

Che-Ming Jack Hu

Doctor of Philosophy

University of California, San Diego, 2011

Professor Michael J. Heller, Chair
Professor Liangfang Zhang, Co-Chair

Therapeutic Nanoparticles have shown significant impact in the field of medicine, particularly in anticancer drug delivery. Prolonged circulation time, functionalization with tumor-targeting ligands, and encapsulation of multiple drug types are among the key features of nanoparticles that make them desirable anticancer drug carriers. This dissertation will focus on these three major features of therapeutic nanoparticles and provide novel improvements in these areas.

The first area of research is multi-drug coencapsulation, where precise control over drug-to-drug ratio has a major impact on the particles' therapeutic efficacy. A drug-polymer conjugate system is used to overcome the intrinsic differences in the physicochemical properties of different drug molecules. By adapting metal alkoxide chemistry, we synthesize highly hydrophobic drug-poly-l-lactide (drug-PLA) conjugates, of which the polymer has the same chain length while the drug may differ. These drug-polymer conjugates are then encapsulated into lipid-coated polymeric nanoparticles through a single-step nanoprecipitation method. Using doxorubicin (DOX) and camptothecin (CPT) as two model chemotherapy drugs, various ratios of DOX-PLA and CPT-PLA conjugates are loaded into the nanoparticles with over 90% loading efficiency. The resulting nanoparticles are uniform in size, size distribution and surface charge. The loading yield of DOX and CPT in the particles can be precisely controlled by simply adjusting the DOX-PLA**:**CPT-PLA molar ratio. Cellular cytotoxicity results show that the dual-drug loaded nanoparticles are superior to the corresponding cocktail mixtures of single-drug loaded nanoparticles. This dual-drug delivery approach offers a solution to the long-standing challenge in ratiometric control over the loading of different types of drugs onto the same drug delivery vehicle.

The second area is nanoparticle functionalization for tumor-targeted delivery. we synthesize anti-CEA half-antibody conjugated lipid-polymer hybrid nanoparticles and characterize their ligand conjugation yields, physicochemical properties, and targeting ability against pancreatic cancer cells. Under the same drug loading, the

half-antibody targeted nanoparticles show enhanced cancer killing effect compared to the corresponding non-targeted nanoparticles. The half-antibody approach offers the advantage of reduced ligand size, site-specific conjugation, and easy accessibility over existing functionalization approaches.

The third area of research presented herein is a novel nature-inspired approach to camouflage nanoparticles for long systemic circulation. A top-down approach in coating biodegradable polymeric nanoparticles with natural erythrocyte membranes is reported. The structure, size and surface zeta potential, and protein contents of the erythrocyte membrane-coated nanoparticles were verified using transmission electron microscopy, dynamic light scattering, and gel electrophoresis respectively. Mice injections with fluorophore-loaded nanoparticles revealed superior circulation half-life by the erythrocyte-mimicking nanoparticles as compared to control particles coated with the state-of-the-art synthetic stealth materials. Biodistribution study revealed significant particle retention in the blood 72 hours following the particle injection. The translocation of natural cellular membranes, their associated proteins and the corresponding functionalities to the surface of synthetic particles represents a novel approach in nanoparticle functionalization.

The developments on these three areas are compatible with one another and could be integrated as one multifunctional nanoparticle platform. Each of these features aims to target a distinctive barrier in cancer drug delivery.

Chapter 1 Introduction

1.1 Barriers in Cancer Drug Delivery

Effective drug delivery is a key factor toward better cancer treatment. Inefficient drug delivery leads to poor tumor response, causes severe side effects, and gives rise to the notorious cancer drug resistance. Since anticancer drugs are typically toxic toward healthy proliferating cells as well, drug dosage must be restricted to avoid potentially lethal side effects. Therapeutic efficacy of such restricted drug dosage can be further diminished by factors such as limited systemic circulation lifetime, undesirable biodistributions, non-specific cellular uptake, and poor tumor vascularity (1). As a result, each course of chemotherapy typically induces partial treatment, which subjects the surviving cancer cells to a selective pressure that favors mutations toward drug resistance. Drugs that show favorable initial response are often

rendered ineffective following repeated administrations, and the relapsed tumor would become much more difficult to treat. To address this serious clinical challenge, research efforts are being undertaken to develop potent therapeutics that can be efficiently delivered to cancers. Under such efforts, drug-loaded nanoparticles (NPs) have emerged as a powerful and versatile carrier platform for improving the delivery efficiency and therapeutic efficacy of chemotherapeutics.

To effectively treat cancers and minimize the effect of cancer drug resistance, high doses of potent therapeutics need to be safely delivered to tumoral sites. Such feat is difficult for small-molecule anticancer drugs, which face numerous barriers as they travel from the point of intravenous administration and to their intended diseased destination. These barriers can be classified into three separate levels: the physiological barrier, the cellular barrier, and the molecular barrier. On the physiological level, small-molecules drugs are rapidly cleared upon systemic injection from plasma degradation (2-4), reticuloendothelial system (RES) uptake (5, 6), and renal filtration (7-9). Because of their poor pharmacokinetics and the short circulation, the majority of administered drugs simply cannot stay in the circulation long enough to reach the tumor. Therefore a major requirement for cancer drug delivery is to prolong the *in vivo* residence time of therapeutic compounds.

On the cellular level, the cellular membrane of cancer cells presents a major barrier to entry. Anticancer drugs typically rely on passive diffusions and membrane translocators to cross the cellular membrane, but these entry mechanisms preclude bulky and polar drugs from penetration (10, 11). In addition, the presence of

membrane bound drug-efflux pumps, which are frequently overexpressed in drug resistant cancer cells (12, 13), actively vacuums drug molecules from the intracellular to the extracellular space. Effective drug delivery needs to shuttle the drugs to the cellular cytoplasm and overcome these membrane barriers.

Lastly, major barriers exist on the molecular level in cancers, which can often survive drug-inflicted damaged in a particular pathway by activating and strengthening the alternative pathways. Such complexity of cancer biology can be likened to "webs of interconnected routes with multiple redundancies" (14), in which single-drug therapies and their one-dimensional action mechanisms are usually inadequate. Frequent mutations prompt the emergence of chemoresistance. Many of these mutations have been identified, including compromised apoptotic signaling, enhanced damage repair mechanisms, increased drug metabolism, altered drug targets, and upregulation of drug-efflux pumps (15). It is, therefore, important to attack cancer cells through multiple pathways in order to minimize the possibility that the cells could acquire a favorable mutation and survive the treatment. To increase therapeutic efficacy, the treatment should possess multiple modes of mechanisms so it could increase the evolutionary hurdle for the cancer cells to acquire drug resistance phenotypes.

A promising way to overcome all the aforementioned barriers is to associate anticancer drugs with NPs. In the last a few decades, the advancement of nanotechnology has made possible the synthesis of nanoscale, biocompatible and biodegradable drug delivery vehicles. Many types of nanocarriers including

liposomes, solid lipid NPs and polymeric NPs have been developed to deliver a variety of drugs (16-18). These nanocarriers have demonstrated desirable drug delivery characteristics such as prolonged systemic circulation lifetime, reduced non-specific cellular uptake, targeting abilities, controllable drug release, and multidrug encapsulation for combinatorial treatment. Recently, NPs with a size range of 50~150 nm are emerging as a promising drug delivery platform for cancer treatment as a number of NP-based cancer drugs are showing up on the market and in clinical trials (19). Numerous chemotherapeutic drugs, including many that are otherwise insoluble in the blood, have been successfully encapsulated in NPs. Other features such as

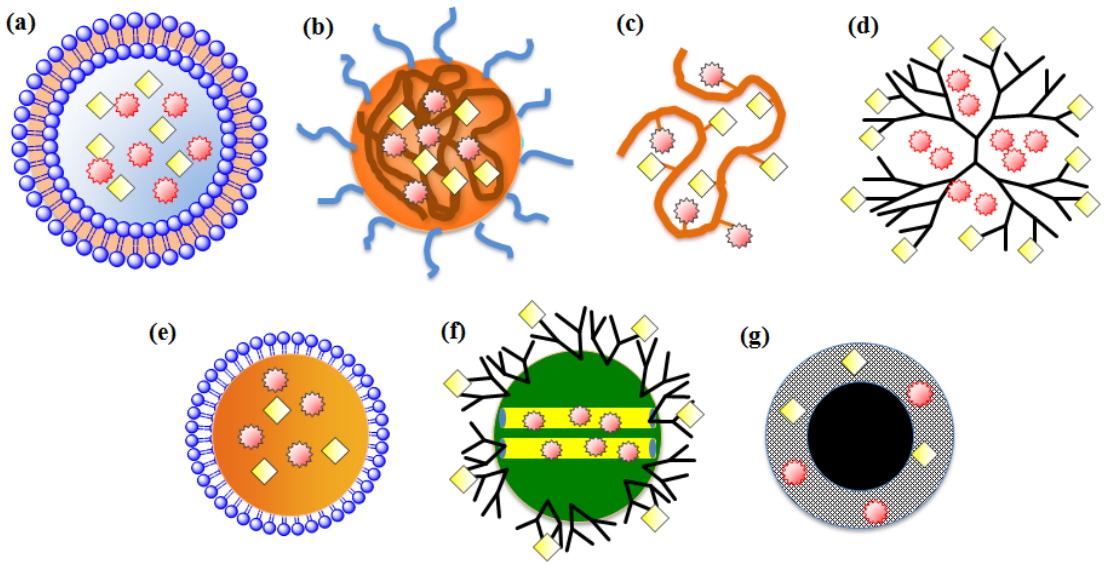


Fig. 1.1. Schematic illustration of nanoscale drug carriers (a) liposome, (b) polymeric micelle, (c) polymer-drug conjugate, (d) dendrimer, (e) oil nanoemulsion, (f) mesoporous silica nanoparticle, and (g) iron oxide nanoparticle.

functionalization with tumor-targeting ligands and co-encapsulation of multiple therapeutics have also been implemented on nanoparticle platforms. This chapter will provide a perspective on the strengths of NPs in improving cancer drug delivery. Illustrations of several types of nanoparticles can be found in figure 1.1.

1.2 Nanoparticles for Effective Cancer Drug Delivery

1.2.1 Prolonged Drug Systemic Circulation Lifetime

Nanoscale particles can break down the physiological barrier in cancer drug delivery by extending the circulation time of small-molecule drugs and enabling passive targeting to tumors. NPs have excellent pharmacokinetics that allow them to take advantage of the leaky vasculatures near the tumoral environment. Tumor vessels are highly abnormal because they lack adequate pericyte coverage and contain large fenestrations. This abnormal porosity gives rise to the "enhanced permeability and retention" (EPR) (20-22) effect by which 50-150 nm therapeutic NPs can escape from tumor capillaries and accumulate in the extracellular tumor matrix. Due to the lack of well developed lymphatic drainage in tumors, NPs that enter the environment are better retained (Fig. 1.2). The EPR effect, however, has negligible benefit for systemically administered free anticancer drugs because of their short circulation lifetime. These small molecule drugs are rapidly removed from the blood by non-specific cellular uptake, immune opsonization, plasma degradation, glomerular filtration and hepatic clearance. In general, small molecule anticancer drugs are

cleared from the blood within hours or shorter after administration. Several NP formulations have been use to improve the pharmacokinetic profiles of anticancer drugs.

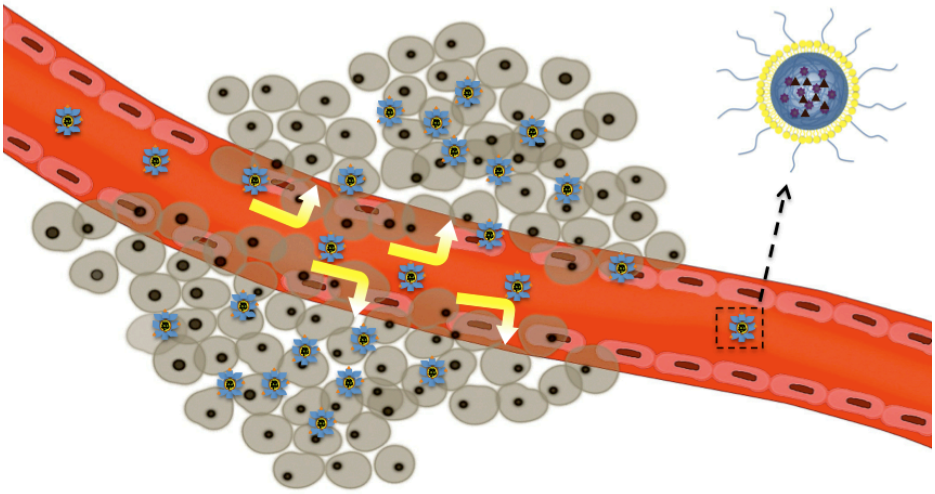


Fig. 1.2. Schematic illustration of the enhanced permeation and retention (EPR) effect in solid tumors. Leaky vasculature and poor lymphatic drainage cause enhanced permeation and retention of nanoscale particles. Nanoparticles that are long-circulating can maximize tumoral uptake through EPR effect.

Early attempts to prolong drug systemic circulation using liposomes, spherical lipid vesicles consisting of a bilayered lipid membrane (23), were met with marginal success. By loading drugs to the hydrophobic lipid membranes or the aqueous interior of liposomes, the drug payloads were shielded from renal filtration and plasma degradation but the liposomes failed to escape from the uptake by the

reticuloendothelial system (RES) such as monocytes and macrophages. Such RES uptake led to rapid removal of the liposomal drugs from the blood. The development of stealth NPs was a major breakthrough in prolonging circulation time while minimizing non-specific cellular uptake. These long-circulating NPs were typically coated with a layer of polyethylene glycol (PEG), which is a synthetic hydrophilic polymer. The PEG coating forms a hydration layer that retards RES recognitions by sterically inhibiting hydrophobic and electrostatic interactions with plasma proteins. Many studies characterized the effects of PEG length and density on NP systemic circulation time and biodistributions (24-26). It has been reported that NPs coated by PEG with a molecular weight of 2~5 kDa give desirable circulation profile for medical applications. It has also been reported that NP size significantly affects their *in vivo* delivery performance. A particle diameter between 50 to 150nm is optimal for drug retention and tumor extravasation (27, 28).

Clinical studies have revealed a striking circulation lifetime difference between free drugs and their NP-encapsulated counterparts. In a detailed review, Gabizon et al. have compared the pharmacokinetics between free doxorubicin (Dox) and PEGylated liposomal Dox (Doxil) (29). Doxil showed improved pharmacokinetic profiles in both human and animal studies. For a 50 mg/m^2 dose injection in human, drug availability of Doxil in blood represented by the area under the concentration (AUC)-time curve was about 300-fold as high as free Dox. More importantly, the enhanced drug retention in the blood was translated to higher and more preferential tumor uptake. For example, in a study in AIDS-related Kaposi's sarcoma, patients

treated with Doxil showed 5- to 11-fold higher drug concentration in skin tumor lesions compared to those treated with free Dox. The lesions also contained 10- to 15-fold higher drug concentration than that in adjacent normal skin, suggesting passive targeting due to EPR effect (30, 31). Visualization of radiolabeled PEGylated liposomes further confirmed their ability to localize at tumor sites. Other types of PEGylated NP systems have shown similar advantages in preclinical studies. By prolonging the circulation time, NPs can more effectively extravagate out of the tumor vasculatures and facilitate preferential drug delivery.

1.2.2 Targeted Drug Delivery

Passive targeting through EPR effect has been best observed in small and well vascularized tumors. In poorly vascularized tumors such as that of colon and pancreas, passive tumor accumulation is often inadequate. Also, vessel permeability might differ within a single solid tumor, resulting in non-uniform drug profusion and incomplete cancer treatment. This limitation has motivated enormous efforts in achieving active targeting through ligand-receptor interactions. Targeting ligands such as antibodies, aptamers, peptides and carbohydrates can be covalently conjugated to NP surfaces. Depending on the size of the NPs and the ligands, tens to hundreds of targeting ligands can be incorporated to each NP to enable multivalent targeting ability that enhances the overall strength of NP binding to the target tumor cells.

One common approach in preparing targeted NPs takes advantage of the well-known molecular recognitions in antibody-antigen binding. Certain antigens are overexpressed in specific cancer types and antibody-modified NPs have shown improved accumulation at those tumor sites. For instance, anti-HER2 immunoliposomes yielded 700-fold higher drug uptake compared to non-targeted liposomes in HER2-overexpressing breast tumors (32). Other antibodies that have been examined for NP cancer targeting include CC52 antibody-modified liposomes against colon adenocarcinoma (33), anti-CD19 for B cell lymphoma (34), and 34A antibody for metastatic lung cancer (35).

Because antibodies are relatively large (~150 kDa in molecular weight), their conjugation often results in poor size control and reduced stealth capability. These shortcomings led to the emergence of alternative targeting ligands. Such ligands include variations of whole antibodies such as Fab fragments (35) and single chain variable fragments (36), growth factors and nutrients whose receptors are overexpressed in cancer cells (37, 38), RNA-based aptamers (39), and peptides such as RGD and LyP-1 that target tumor vasculatures (40-42). The small physical dimension of these alternatives enables high ligand density and more effective multivalent targeting without compromising the particle's circulation time. For example, in an *in vivo* study that compared the performance of antibody-liposomes to their Fab counterparts, the Fab-liposomes showed a 6-fold increase in circulation half-life and a 2-fold increase in tumor retention (35).

1.2.3 Endocytic Uptake of Drugs

Not only can NPs enhance drug accumulation at tumor sites, they can also directly break down the cellular barrier in cancer drug delivery and deliver a high dose of drugs to the cytosolic compartment of cancer cells. Small-molecule drugs rely on passive diffusion or membrane translocators to enter their cellular targets. This process can be extremely inefficient depending on the size and polarity of the drug molecules. In addition, in drug-resistant cancer cells, which often overexpress membrane-bound drug efflux pumps, drugs that diffuse through the cellular membrane are rapidly vacuumed out of the cells before they can take effect. In contrast, therapeutic NPs can bypass the membrane barrier and the drug efflux pumps as they are internalized through endocytosis (43, 44). Once being engulfed by the plasma membrane, NPs are transported by endosomal vesicles before unloading their drug payloads. Thus drug molecules are released farther away from the membrane-bound drug efflux pumps and therefore are more likely to reach and interact with their targets. Numerous studies have shown that NP encapsulation results in better drug effectiveness against cancer cells. For example, the liposomal formulation of digoxin showed higher intracellular uptake and enhanced efficacy compared to free digoxin (45). In another study, it was demonstrated that Dox encapsulated in polyalkylcyanoacrylate NPs was more cytotoxic to P388 resistant cells than free Dox. The IC50 of Dox-loaded NPs was 800 ng/mL while that of free Dox was 20000 ng/mL. Similar efficacy enhancement has been observed for many other therapeutic NP platforms (45-48), suggesting that endocytic transport is a viable strategy to cross

the cellular barrier in cancer drug delivery (Fig. 1.3.). The presence of targeting ligands on NPs can further aid the crossing of the cellular barrier by promoting receptor-mediated endocytosis. In the aforementioned study that examines the efficacy of anti-HER2 immunoliposomes against HER2 overexpressing breast cancers (32), the anti-HER2 liposomes were found mostly in the cytoplasm of cancer cells following intravenous injection whereas the bare liposomes accumulated extracellularly or in macrophages. The study demonstrated superior cellular delivery by targeted NPs.

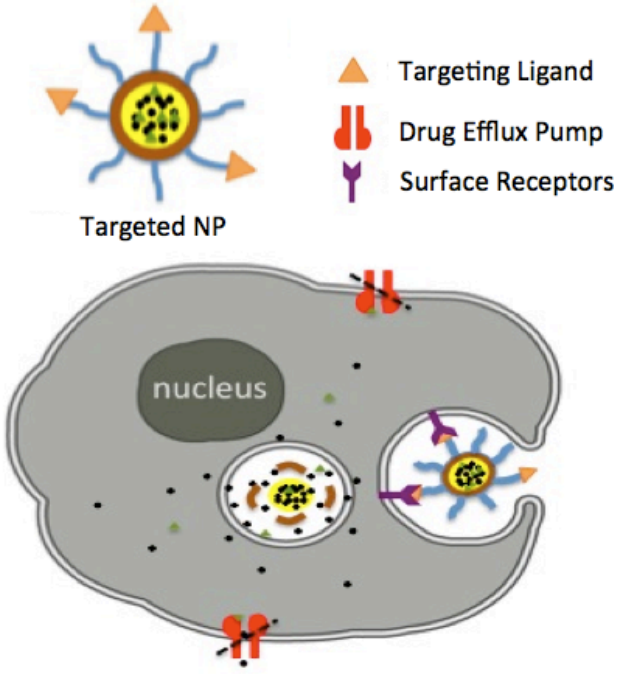


Fig. 1.3. Schematic illustration of NP endocytosis to cross the membrane barrier for cellular entry.

1.2.4 Co-delivery of Multiple Therapeutic Agents in Combination

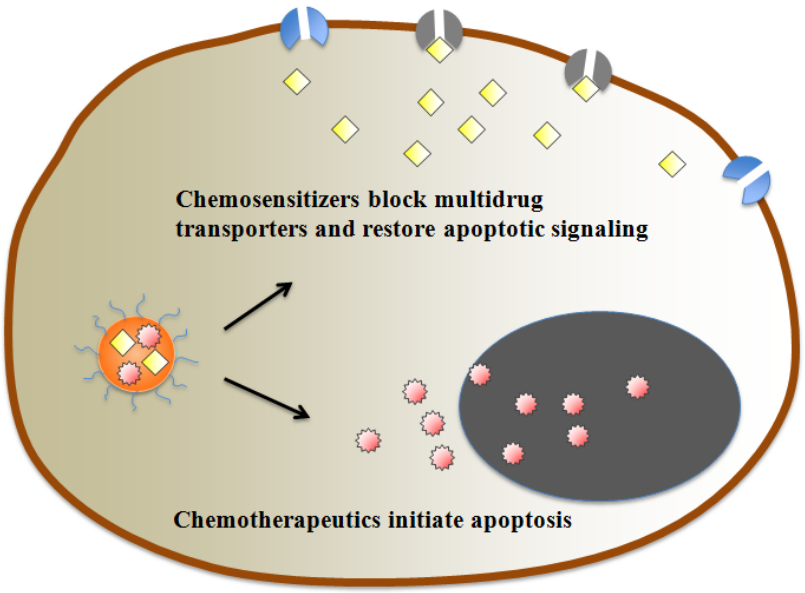
The molecular barrier in cancer drug delivery is manifested in the emergence of cancer drug resistance. Cancer cells often time acquire defense mechanisms against the presence of therapeutic compounds. Combination chemotherapy has long been adopted as the standard of care to combat the molecular barrier in cancers. It is generally acknowledged that through the proper drug combination the treatment can promote synergistic actions, improve target selectivity, and deter the development of cancer drug resistance (49). Advances in nanotechnology have opened up unprecedented opportunities in novel combination strategies. Recently, nanocarriers are gaining increasing attention for their ability to co-encapsulate multiple therapeutic agents and to synchronize their delivery to the diseased cells. One distinctive advantage of NP-based combination therapy over traditional cocktail combinations is NPs' ability to maintain the synergistic drug-to-drug ratio *in vivo*. Drug-to-drug ratio has been found to govern the efficacy of combination treatments. Multiple studies suggest that the degree of synergism and antagonism of a combination therapy is highly dependent on the relative concentrations between the combined drugs (50, 51). By unifying the pharmacokinetics of their cargoes, combinatorial nanoparticles open the avenue to co-delivering multiple drugs at a predetermined ratio that maximizes the combination efficacy. Currently, dual-drug liposomes with precise molar ratios have been prepared, and their superiority over traditional combination therapy are highlighted by the clinical trials of CPX-351, a 5:1 cytarabine and daunorubicin formulation for acute leukemia treatment (52-54), and CPX-1, a 1:1 irinotecan and

floxuridine formulation for colorectal cancer treatment (55). These liposomes demonstrate the ability to maintain the synergistic drug ratios *in vivo* and are more effective than the cocktail administration of the free drugs.

By co-encapsulating chemosensitizing agents, combinatorial NPs have also shown the ability to reverse multidrug resistance (MDR) phenotypes in cancer cell lines (Fig. 1.4). For instance, Soma et al. have encapsulated cycloporin A (CyA), a compound that binds directly to P-glycoprotein (P-gp) drug efflux pump and inhibits its activity, together with Dox in polyalkylcyanoacrylate NPs (56). In preparing the combinatorial NPs, CyA and Dox were mixed with the isobutylcyanoacrylate monomers during the emulsion polymerization process. As the NPs were formed, CyA was absorbed onto the particle surface whereas Dox was embedded in the polymeric core. Activities of both CyA and Dox were preserved as the combinatorial NPs showed higher growth inhibition on P388 Dox-resistant cells as compared to the NPs loaded with Dox alone. The measured IC50 value of CyA-Dox-loaded NPs and Dox-loaded NPs was 450 ng/mL and 800 ng/mL, respectively. In addition, the study also demonstrated that NPs enabled the synergistic effect between CyA and Dox because free CyA in solution failed to improve the growth inhibition ability of Dox-loaded NPs.

Curcumin is another P-gp modulator that has been co-encapsulated in NPs with anticancer drugs (57). Curcumin is a naturally occurring compound that downregulates P-gp expression and facilitates apoptotic signaling. Because of its hydrophobic characteristic, curcumin was readily encapsulated in oil-in-water

nanoemulsions along with paclitaxel. Results from western blotting revealed that the P-gp expression in paclitaxel-resistant SKOV3 human ovarian adenocarcinoma cells was significantly reduced after curcumin nanoemulsion treatment. The downregulation of P-gp contributes to the higher cytotoxicity of the combinatorial nanoemulsions, whose IC50 is 1.8 fold less than that of the nanoemulsions loaded with paclitaxel alone. Further study found that the combinatorial treatment inhibited NFkB, a transcription factor that induces the expression of anti-apoptotic proteins and is closely related to paclitaxel resistance (58). These findings suggest that therapeutic NPs co-delivering chemo-sensitizing agents and anticancer drugs can effectively suppress cancer drug resistance by resensitizing the MDR cells to chemotherapeutic



treatment.

Fig. 1.4. Schematic presentation of combinatorial nanoparticles containing chemosensitizers and chemotherapeutics against MDR of a cancer cell.

Not only can modulators of P-gp or other multidrug transporters be co-delivered with anticancer drugs by therapeutic NPs, compounds that modify other cellular activities can also be co-delivered to restore the mutated biochemical processes in drug resistant cells. For example, ceramide is a secondary messenger in the signaling cascade of the apoptotic pathway and it has been loaded into therapeutic NPs to overcome MDR (59). Environmental stress such as cytotoxic agents elevates the intracellular ceramide level, which then promotes cell death by apoptosis. Some MDR tumors, however, exhibit a high level of glucosylceramide synthase that metabolizes ceramide to its inactive glycosylated form. These tumors are thus less likely to initiate the apoptotic process when treated with chemotherapeutic agents. In an attempt to revive the dysfunctional apoptotic signaling, ceramide was co-encapsulated with paclitaxel in poly(ethylene oxide)-poly(epsilon caprolactone) (PEO-PCL) NPs. It was found that the combinatorial NPs showed 100% cellular growth inhibition against SKOV3 paclitaxel-resistant cells at the IC50 dose of, paclitaxel. This higher cytotoxicity translated to a 100-fold increase in chemosensitization of the co-delivery therapeutic NPs. Apoptotic activity analysis and western blotting study further revealed that the enhanced therapeutic efficacy was indeed due to the restoration of the defunct apoptotic pathway, indicating that drug resistance was reversed. A summary of combinatorial NP formulations that overcome the molecular barrier in cancer treatment and reverse drug resistance can be found in Table 1.1.

Table 1.1. Selected examples of combinatorial nanoparticle formulations containing chemotherapeutics and chemosensitizers.

Nanocarrier Platform	Chemo-Therapeutic	Chemosensiting Agent	Indication	Status	Refs
Liposome	Topotecan	amlodipine	Leukemia	*in vivo*	(60)
Liposome	Vincristine	quinacrine	Leukemia	*in vivo*	(61)
Liposome	Paclitaxel	tariquidar	Ovarian cancer	*in vitro*	(62)
Liposome (transferrin-conjugated)	Doxorubicin	verapamil	Leukemia	*in vitro*	(63)
Liposome (cationic)	Doxorubicin	MRP-1 and BCL2 siRNA	Lung Cancer	*in vitro*	(64)
Cationic core-shell nanoparticle	Paclitaxel siRNA	BCL2- siRNA	Breast cancer	*in vitro*	(65)
PLGA-PEG nanoparticle	Vincristine	verapamil	Breast Cancer	*in vitro*	(66)
PLGA-PEG-biotin nanoparticle	Paclitaxel	tariquidar	Various cancer types	*in vivo*	(67)
PLA-PEG-biotin nanoparticle	Paclitaxel	P-gp siRNA	Various cancer types	*in vivo*	(68)
Polyalkylcyanoacrylate nanoparticle	Doxorubicin	Cyclosporine A	Various cancer types	*in vitro*	(56)
Oil nanoemulsion	Paclitaxel	curcumin	Ovarian Cancer	*in vitro*	(69)
Mesoporous silica nanoparticle	Doxorubicin	BCL2-siRNA	Ovarian Cancer	*in vitro*	(70)

1.3 Challenges in Nanoparticle Drug Delivery

Therapeutic NPs are emerging as a safer and more effective drug delivery option as compared to their small molecule chemotherapy counterparts. They have shown numerous favorable features including long systemic circulation lifetime, targeting ability, cellular internalization through endocytosis, and co-delivering multiple therapeutic agents. These desirable features make therapeutic NPs highly promising in combating cancer drug resistance.

1.3.1 Challenges in Multi-drug Coencapsulation in Nanoparticles

In combination chemotherapy, drug ratios govern whether the combined therapeutics can be synergistic or antagonistic. Precise control over the drug-to-drug ratios, therefore, is of major importance in NP multi-drug coencapsulation. Control over drug ratios have been achieved on the liposomal platform as in the case of CPX-351 and CPX-1. Ratiometric control was made possible in these liposomal formulations through adjustment over the preparation parameters such the lipid composition, drug concentration during lipid film hydration and liposome incubation process, and incubation time. In other NP platforms, however, such control has yet to be achieved. In polymeric NPs, for instance, drug co-encapsulation through non-covalent physical entrapment leads to batch-to-batch variability in drug concentrations. Developing a scheme for the facile assembly of ratiometrically

controlled multi-drug NPs would have significant impact on NP-based combination therapy.

1.3.2 Challenges in Tumor-targeted Nanoparticles

Even though the antibody conjugations are widely adopted in various biomedical applications, most techniques are based on randomized modifications that could block the binding sites and compromise the targeting efficiency. Engineered recombinant fusion proteins, such as single-chain antibody, affibody, and variants of antibody fragments, are an alternative to achieve regioselective targeting ligand conjugation (71-74), but these engineered proteins can cost more than 10 times as much as the typical antibodies and are very difficult to access. Often time these recombinant proteins need to be custom made, and the process can be extremely time-consuming. A more accessible and economical approach in site-specific conjugation of targeting ligands would significantly increase the applicability of tumor-targeted NPs.

1.3.3 Challenges in Long-circulating Nanoparticle

PEG is currently the gold standard for the stealth moiety, and it is present in many FDA-approved products. However, concerns and limitations of PEG such

as its non-biodegradability, immunological responses, and the toxic side products that accompany its synthesis, have motivated the search for safer and more compatible substitutes (75). Of the utmost concern is the emergence of anti-PEG antibodies that have been observed in approximately 25% of Americans (76, 77). One study has shown that repeated dosing with PEGylated NPs resulted in accelerated blood clearance of the particles (78). Such observations raise concerns over the ubiquitous use of PEG and call for the need for novel, non-immunogenic approach in prolonging NP circulation half-life. Ideally stealth moieties can be developed to mimic our bodies' endogenous materials to evade the immune surveillance.

Chapter 1 is based, in part, on the material as it appears in Current Drug Metabolism, 2009, Che-Ming Hu and Liangfang Zhang, and, in part, on the material submitted for publication as it may appear in Biochemical Pharmacology 2011, Che-Ming Hu and Liangfang Zhang. The dissertation author was the primary investigator and co-author of these papers. The remainder of this dissertation will focus on novel drug delivery systemic based on polymeric NP platforms to address the aforementioned challenges in multi-drug coencapsulation, tumor targeting functionalization, and long in-vivo circulation.

Chapter 2 Polymeric Nanoparticles with Precise Ratiometric Control over Drug Loading

2.1 Introduction

Nanoparticulate drug delivery systems have become increasingly attractive in systemic cancer drug delivery because of their ability to prolong drug circulation half-life, reduce non-specific uptake, and better accumulate at the tumors through enhanced permeation and retention (EPR) effect or active targeting.(21, 79-83) As a result, several therapeutic nanoparticles such as Doxil® and Abraxane® are used as the frontline therapies in clinics. But despite the advancement in nanoparticle drug delivery, most research efforts focus on single drug encapsulation whereas delivering multiple drugs with a single vesicle remains largely unexplored. Combination chemotherapy has shown superior clinical therapeutic efficacy compared to single-drug therapy, particularly in retarding the development of cancer chemoresistance.(84,

85) It has been frequently observed that the cancer cells acquire defense mechanisms by over-expressing drug efflux pumps, increasing drug metabolism, enhancing self-repairing ability or expressing altered drug targets,(15, 86) resulting in diminishing efficacy and ultimately treatment failures. Many drugs have been routinely administered in combination to improve the treatment effectiveness.(87-89) However, current combination regimens are limited by the distinct pharmacokinetics and biodistribution of different drug molecules and offer little flexibility for treatment optimization.

One of the biggest motivations behind nanoparticle-based combination therapies is their ability to unify the pharmacokinetics and biodistribution of different drug molecules, thereby enabling dosage optimization *in vivo*. By delivering multiple therapeutic agents to the target cells simultaneously, the multi-drug delivery nanoparticles can promote drug synergism and pave the way to precision design and tailoring in cancer chemotherapeutics. Several strategies have been employed to co-encapsulate multiple drugs into a single nanocarrier, including physical loading into the particle core,(56, 90, 91) chemical conjugation to the particle surface,(92) and covalent linkage to the polymer backbone prior to nanoparticle synthesis.(93-96) However, controlling the ratios of different types of drugs in the same nanoparticles remains a major challenge because of factors such as steric hindrance between the different drug molecules and the polymer backbones, batch-to-batch heterogeneity in conjugation chemistry, and variability in drug-to-drug and drug-to-polymer interactions. One approach to address these issues is to covalently conjugate dual

drugs using a hydrolysable linker and then encapsulate the drug-drug conjugates into nanoparticles for co-delivery.(97) Despite the success in maintaining the ratio between two drugs with drastically different properties, this linker approach is constrained to small drug-to-drug molar ratio such as 1:1 and thus has limited clinical applicability. Herein, we present a versatile dual-drug encapsulation scheme in which each different drug molecule is linked to an individual polymer backbone that has the same physicochemical properties and nearly the same chain length. These drug-polymer conjugates are subsequently mixed at predetermined ratios for nanoparticle synthesis. The long and sharply distributed polymer chain gives each drug molecule a predominant and uniform hydrophobic property, yielding near 100% drug encapsulation efficiency upon nanoparticle formation.

In this study, we demonstrated the synthesis of drug-polymer conjugates with two different chemotherapeutics, doxorubicin (DOX) and camptothecin.(98) Utilizing ring-opening polymerization of l-lactide, we synthesized DOX and CPT polymer conjugates using metal-amido catalyst, which reacts selectively with hydroxyl groups of the drug molecules to initiate polymerization.(98-100) Using a nanoprecipitation technique (Fig. 2.1), the drug-polymer conjugates were quantitatively loaded into lipid-polymer hybrid nanoparticles at high loading yield and precisely controlled drug ratios. The combinatorial treatment proposed here showed superior efficacy to cocktail therapy *in vitro* and offers a solution to the aforementioned limitations in multi-drug encapsulation into the same nanoparticles. Since this drug-polymer conjugation approach can be generalized to a variety of therapeutic agents, we expect

this combinatorial drug delivery system would set a new paradigm in nanomedicine for different combination therapies.

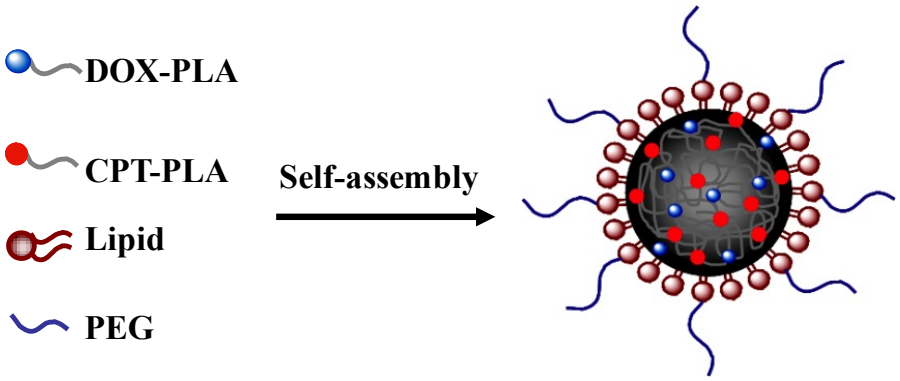


Fig. 2.1. Schematic illustration of a dual-drug loaded lipid-polymer hybrid nanoparticle, of which the polymeric core consists of two distinct drug-polymer conjugates with ratiometric control over drug loading.

2.2 Experimental Methods

2.2.1 Materials

L-lactide was purchased from Sigma-Aldrich Co. (Milwaukee, WI), recrystallized three times in ethylacetate and dried under vacuum. L-lactide crystals were further dried inside a glove box and sealed into a glass vial under dry argon and then stored at -20 °C prior to use. 2,6-di-iso-propylaniline (Sigma-Aldrich Co.) and 2,4-pentanedione (Alfa Aesar Co., Ward Hill, MA) were used as received. All other chemicals and anhydrous solvents were purchased from Sigma-Aldrich Co. unless

otherwise specified. Anhydrous tetrahydrofuran and toluene were prepared by distillation under sodium benzophenone and were kept anhydrous by using molecular sieves. The 2-((2,6-diisopropylphenyl)amino)-4-((2,6-diisopropylphenyl)imino)-2-pentene (BDI) ligand and the corresponding metal catalysts (BDI)ZnN($SiMe_3$)$_2$ were prepared inside a glove box following a published protocol and stored at -20 °C prior to use. DOX·HCl was purchased from Jinan Wedo Co., Ltd. (Jinan, China) and used as received. Removal of HCl from DOX·HCl was achieved by neutralizing DOX·HCl solution in water with triethyleamine, after which the solution color changed from red to purple. The free base form of DOX was subsequently extracted with dichloromethane. The organic extract was filtered through anhydrous Na_2SO_4 and dried under vacuum to collect DOX crystals. (S)-(+)-Camptothecine (CPT) was purchased from TCI America and used as received.

2.2.2 Synthesis of 2-((2,6-diisopropylphenyl)amino)-4-((2,6-diisopropylphenyl)imino)-2-pentene (BDI)

Ligand BDI was prepared following a previously published protocol with minor modification.(101) Briefly, 2,6-Di-n-propylaniline (13.0 mmol) and 2,4-pentanedione (6.5 mmol) in the ratio of 2:1 were dissolved in absolute ethanol (20 ml). The mixture solution was acidified with concentrated HCl (0.6 mL) and heated at reflux for 48 h, which resulted in white precipitates. After being cooled to room temperature, the white precipitates were dissolved with dichloromethane and saturated aqueous bicarbonate solution. The orange colored solution was then

extracted and washed with brine three times and filtered through anhydrous Na_2SO_4, followed by being concentrated and precipitated in hexane. The resulting precipitates were collected by filtration, suspended in diethyl ether (20 mL), and washed with saturated aqueous bicarbonate followed by brine. The organic layer was then separated through filtration in the presence of Na_2SO_4 to absorb moisture and then precipitated in hexane as a light brown powder (yield ~ 60%). ^{1}H NMR (JEOL, $CDCl_3$, 500 MHz): δ 12.20 (br, ^{1}H, NH), 7.12 (m, 6H, ArH), 4.83 (s, ^{1}H, Hβ), 3.10 (m, 4H, $CHMe_2$), 1.72 (s, 6H, α-Me), 1.22 (d, 12H, CHMeMe'), 1.12 (d, 12H, CHMeMe′) ppm. ESI-MS (positive): m/z = 419.43 [M+H]+.

2.2.3 Synthesis of (BDI)ZnN(SiMe$_3$)$_2$ Catalyst

Zinc bis-(trimethylsilyl)amide (463 mg, 1.19 mmol) in toluene (20 mL) was added into a solution of BDI (500 mg, 1.19 mmol) in toluene (20 mL). The mixture solution was stirred for 18 h at 80 °C and then the solvent was removed under vacuum to form (BDI)ZnN($SiMe_3$)$_2$ as a light yellow solid, which was recrystallized from toluene at -30 °C to yield colorless blocks (yield ~ 70%).^{1}H NMR (JEOL, C6D6, 500 MHz): δ (br, ^{1}H, NH), 6.9-7.13 (m, 6H, ArH), 4.85 (s, ^{1}H,Hβ), 3.25 (m, 4H, CHMe2), 1.67 (s, 6H, α-Me), 1.1-1.25 (d, 12H+12H=24H, CHMeMe′), 0.08-0.1 (18H, s, $SiCH_3$) ppm.

2.2.4 Ring Opening Polymerization of l-lactide

Following previously published protocols, DOX-PLA and CPT-PLA polymers were synthesized through ring opening polymerization of l-lactide initiated by alkoxy complex of (BDI)ZnN($SiMe_3$)$_2$ in a glove box under argon environment at room temperature. For the synthesis of DOX-PLA, (BDI)ZnN($SiMe_3$)$_2$ (6.4 mg, 0.01 mmol) and DOX (5.4 mg, 0.01 mmol) were mixed in 0.5 mL of anhydrous THF. L-lactide (101.0 mg, 0.7 mmol) dissolved in 2 mL anhydrous THF was added dropwise. After the l-lactide was completely consumed, the crude product was precipitated in cold diethyl ether, yielding DOX-PLA conjugates. The CPT-PLA conjugates were synthesized in the same procedures as the DOX-PLA. These drug-polymer conjugates had a molecular weight of about 10,000 g/mole determined by gel permeation chromatography.

2.2.5 Preparation of Lipid-Coated Drug-Polymer Conjugate Nanoparticles

Lipid-polymer hybrid nanoparticles with polymeric cores consisting of the synthesized drug-polymer conjugates were prepared through a nanoprecipitation method.(102, 103) In detail, 200 μg of egg PC (Avanti Polar Lipids Inc.) and 260 μg of 1,2- distearoyl-sn-glycero-3- phosphoethanolamine-N-carboxy(polyethyleneglycol)-2000 (DSPE-PEG-COOH) (Avanti Polar Lipids Inc.) were dissolved in 4% ethanol and stirred for 3 min. A total of 500 μg of DOX-PLA and CPT-PLA was dissolved in acetonitrile and added dropwise to the lipid solution

while stirring. The solution was then vortexed for 3 min followed by the addition of deionized water (1 mL). Then the diluted solution was stirred at room temperature for 2 h, washed with PBS buffer using an Amicon Ultra centrifugal filter with a molecular weight cutoff of 100 kDa (Millipore, Billerica, MA), and resuspended in 1 mL of PBS. Nanoparticles with different DOX/CPT drug ratios were prepared by adjusting the amount of each type of drug-polymer conjugates while keeping the total polymer weight at 500 μg. The nanoparticle size and surface zeta potential were obtained from three repeat measurements by dynamic light scattering (DLS) (Malvern Zetasizer, ZEN 3600) with a backscattering angle of 173°. The morphology of the particles was characterized by scanning electron microscopy (SEM) (Phillips XL30 ESEM). Samples for SEM were prepared by dropping nanoparticle solution (5 μL) onto a polished silicon wafer. After drying the droplet at room temperature overnight, the sample was coated with chromium and then imaged by SEM. The drug loading yield of the synthesized nanoparticles was determined by UV-spectroscopy (TECAN, infinite M200) using the maximum absorbance at 482 nm for DOX and 362 nm for CPT. No shift in the absorbance peak was observed between the free drugs and their polymer conjugates. Standard calibration curves of both DOX and CPT at various concentrations were obtained to quantify drug concentrations in the nanoparticles.

2.2.6 Cellular Colocalization and Cytotoxicity Studies

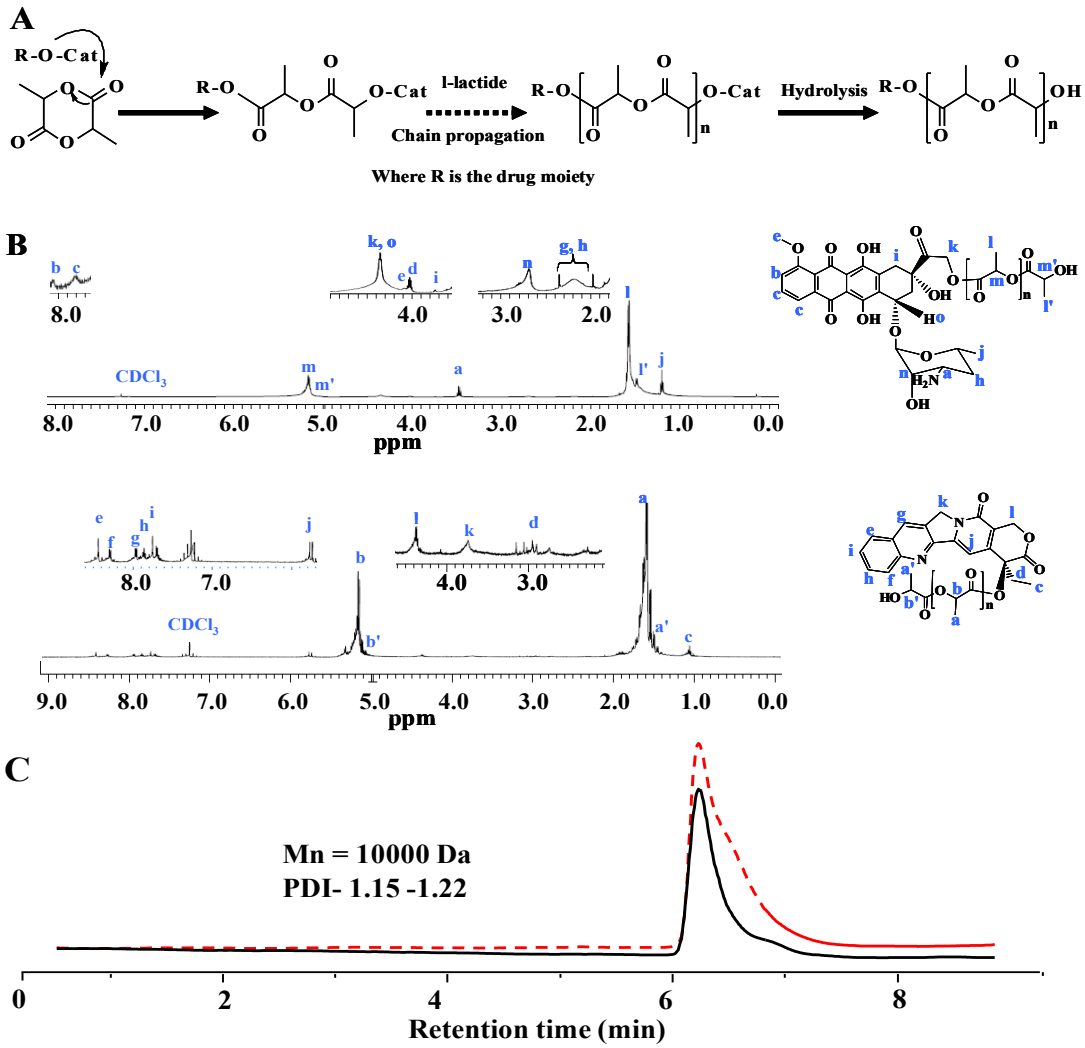
The MDA-MB-435 cell line was maintained in Dulbecco's modification of Eagle's medium (DMEM, Mediatech, Inc.) supplemented with 10% fetal calf albumin, penicillin/streptomycin (GIBCO®), L-glutamine (GIBCO®), nonessential amino acids, sodium bicarbonate, and sodium pyruvate (GIBCO®). The cells were cultured at 37°C and 5% CO_2. For the dual-drug colocalization and cellular internalization study, the cells were incubated with dual-drug loaded nanoparticles for 4 h, washed with PBS, and fixed on a chamber slide for fluorescence microscopy imaging. The cytotoxicity of the dual-drug loaded nanoparticles was assessed using the (3-(4,5-dimethylthiazol-2-yl)-2,5-diphenyltetrazolium bromide (MTT) assay (Promega, Madison, WI). Briefly, the cells were seeded at 25% confluency (~4×103 cells/well) in 96-well plates and incubated with different concentrations of drug loaded nanoparticles for 24 h. The cells were then washed with PBS three times and incubated in fresh media for an additional 72h. MTT assay was then applied to the samples to measure the viability of the cells following the manufacturer's instruction.

2.3 Results and Discussion

2.3.1 Synthesis and Characterization of Drug-Polymer Conjugates

In the study, we used (BDI)ZnN($SiMe_3$)$_2$, a metal-amido complex in which BDI refers to 2-((2,6-diisopropylphenyl)amido)-4-((2,6diisopropylphenyl)-imino)-2-pentene, as a catalyst for the *in-situ* formation of metal-alkoxide with the hydroxyl group of DOX and CPT to initiate the living polymerization of l-lactide and form drug-poly-l-lactide (drug-PLA) conjugates (Fig. 2.2A). The formation of the drug-polymer conjugates was verified by the ^{1}H-NMR spectroscopy, which exhibits all the characteristic proton resonance peaks corresponding to the parent drug molecules. The appearance of the aromatic proton resonance at δ 7.5 to 8.0 ppm in DOX-PLA conjugates (Fig. 2.2B, top panel) and δ 7.5 to 8.5 ppm in CPT-PLA conjugates (Fig. 2.2B, bottom panel) along with the characteristic –CH_3 proton of PLA at δ 1.5 ppm and –CH proton at δ 5.2 ppm confirms the formation of the drug-polymer conjugates. The desired drug-polymer conjugation products were further validated by gel permeation chromatography (GPC) which shows the molecular weight as 10,000 Dalton for both DOX-PLA and CPT-PLA conjugates (Fig. 2.2C). The molecular weight is in accord with the monomer-to-initiator feed ratio which indicates near 100% conversion of the monomers to polymers. Since the formation of metal alkoxide complex is quantitative and the reaction is homogeneous, the reaction proceeded quantitatively such that all monomers were converted into products. Also the molecular weight of the polymer matches that from an earlier study conducted by

Tong *et al*. who used (BDI)ZnN(SiMe$_3$)$_2$ to catalyze the ring opening polymerization



of both DOX and CPT.(98, 100)

Fig. 2.2. Chemical characterization of the drug-polymer conjugates. (A) Schematic description of the living ring-opening polymerization of l-lactide catalyzed by an activated metal alkoxide complex. (B) Qualitative ^{1}H-NMR spectra showing the characteristic proton resonance peaks of DOX-PLA (upper panel) and CPT-PLA (lower panel). (C) Gel permeation chromatograms of DOX-PLA (red dashed line) and CPT-PLA (black solid line).

2.3.2 Synthesis and Characterization of Dual-Drug Loaded Polymeric Nanoparticles

Upon successful synthesis of the drug-polymer conjugates, we used them to prepare lipid-polymer hybrid nanoparticles for dual-drug delivery. Using DSPE-PEG and phospholipids to coat the polymeric nanoparticle core, the resulting lipid-polymer hybrid nanoparticles are highly stable in water, PBS, and serum and have high drug loading yield as the entire polymeric core consists of the drug-polymer conjugates. Moreover, by simply adjusting the DOX-PLA:CPT-PLA molar ratio, dual-drug loaded nanoparticles with ratiometric drug loading of DOX and CPT were prepared. Keeping the total drug-polymer conjugates weight constant at 1mg, we varied the DOX-PLA:CPT-PLA ratio to tune the ratiometric drug loading. The resulting drug-loaded nanoparticles exhibit a unimodal size distribution at ~100 nm with low PDI values (Fig. 2.3). In addition, the particles possess negative surface zeta potential, which is consistent with the DSPE-PEG-COOH coating and serves to prevent the particles from aggregation. The particle size measured by DLS was consistent with the SEM images of the particles (Fig. 2.3).

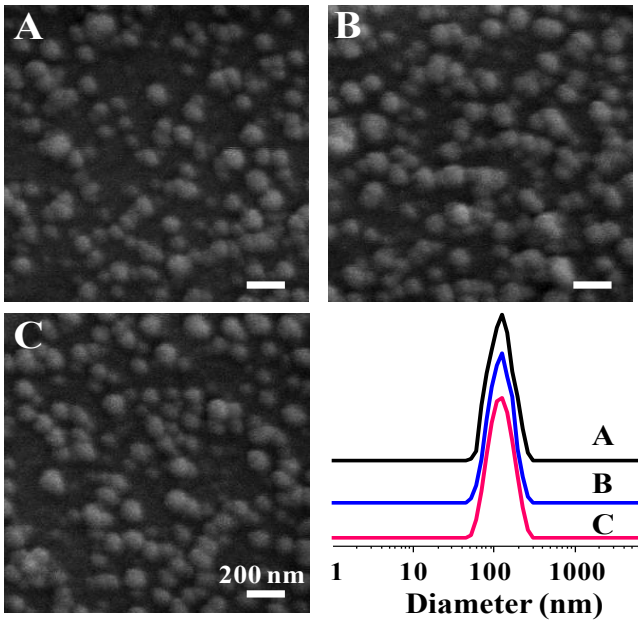


Fig. 2.3. Scanning electron microscopy (SEM) and dynamic light scattering (DLS) measurements showing the morphology and size of lipid-polymer hybrid nanoparticles with the polymer cores consisting of: (A) DOX-PLA conjugates, (B) CPT-PLA conjugates, and (C) DOX-PLA and CPT-PLA conjugates with a molar ratio of 1:1.

2.3.3 Ratiometric Control Over Dual-Drug Loading

Following the physicochemical characterization of the particles, we next examined the drug loading efficiency in these drug-polymer conjugate nanoparticle systems. We prepared various formulations of the nanoparticles with different ratios of drug-polymer conjugates and found that, in all cases, over 90% of the conjugates were encapsulated into the nanoparticles (Fig. 2.4). No change in loading efficiency was observed when DOX-PLA and CPT-PLA conjugates were loaded in combination

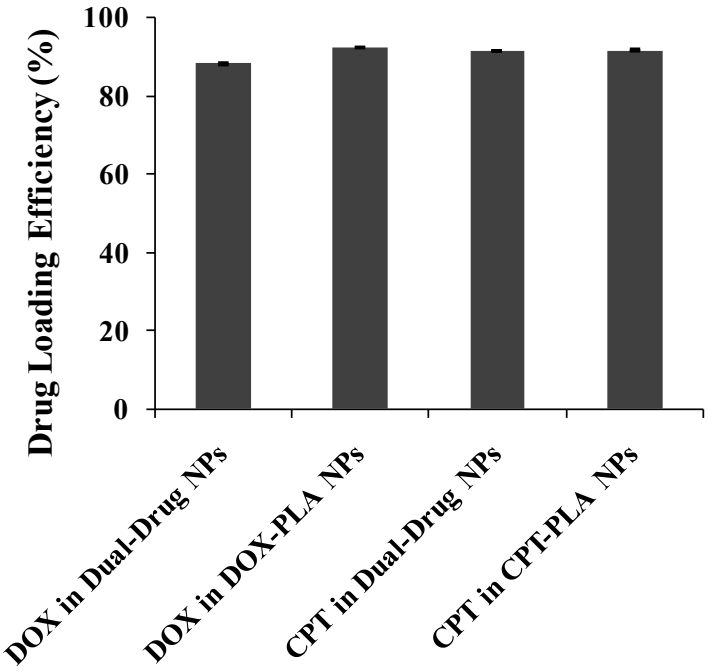


Fig. 2.4. Quantification of DOX and CPT loading efficiency in dual-drug loaded nanoparticles (containing both DOX-PLA and CAP-PLA) and single-drug loaded nanoparticles (containing DOX-PLA or CPT-PLA), respectively. NPs: nanoparticles.

or separately, presumably due to the fact that the long and sharply distributed PLA polymer chain gives each drug molecule a predominant and uniform hydrophobic property. Therefore, they were completely encapsulated and stabilized by the lipid and the lipid-PEG layers in the lipid-polymer hybrid nanoparticle system. Furthermore, we varied the DOX-PLA: CPT-PLA molar ratios from 1:1, to 3:1 and to 1:3, while keeping the total drug-polymer conjugates mass constant. It was found that the final loading yields of DOX and CPT in the dual-drug loaded nanoparticles were highly consistent with the initial DOX-PLA: CPT-PLA molar ratios (Table 2.1).

These results further confirm that this approach enables one to encapsulate different types of drugs to the same nanoparticles with ratiometric control over drug loading.

Table 2.1. Characteristic features of the lipid-coated drug-polymer conjugate nanoparticles.

DOX-PLA/CPT-PLA molar ratios	1:0	0:1	1:1	3:1	1:3
Particle size (nm)	100±2				
Particle PDI	0.17~0.22				
Particle zeta potential (mV)	-47±2				
DOX loading (μM)	47.8±0.2	0	24.0±0.1	35.8±0.2	12.0±0.8
CPT loading (μM)	0	48.2±0.1	24.4±0.1	12.3±0.1	36.2±0.2

2.3.4 Dual-Drug Colocalization and Cellular Internalization

Upon verifying the excellent drug loading efficiency in the present system, we then examined whether the different drug-polymer conjugates are loaded into the same nanoparticles as opposed to forming two different particle populations. To this end, we studied the colocalization of the two drug molecules and their internalization into cells through fluorescence microscopy. Since DOX is also a highly fluorescent molecule, the DOX-PLA conjugates can be identified from DOX's characteristic fluorescence wavelength (excitation/emission = 540 nm/600 nm). To visualize CPT-

PLA, we attached a fluorescent probe, 6-((7-amino-4-mehylcoumarin-3-acetyl) amino) hexanoic acid succinimidyl ester (excitation/emission = 353 nm/442 nm), to the hydroxyl end of the CPT-PLA. The nanoparticle size and size distribution was well controlled before and after fluorophore conjugation in case of CPT-PLA-probe, which further confirms that the nanoparticle formulation with lipid coatings were highly stable and reproducible. Figure 2.5 shows the fluorescence microscopy images that exhibit the colocalization of the DOX-PLA and the CPT-PLA-probe. The colocalization study indicates that no segregation between the two types of drug-polymer conjugates occurs and each particle contains both DOX and CPT.

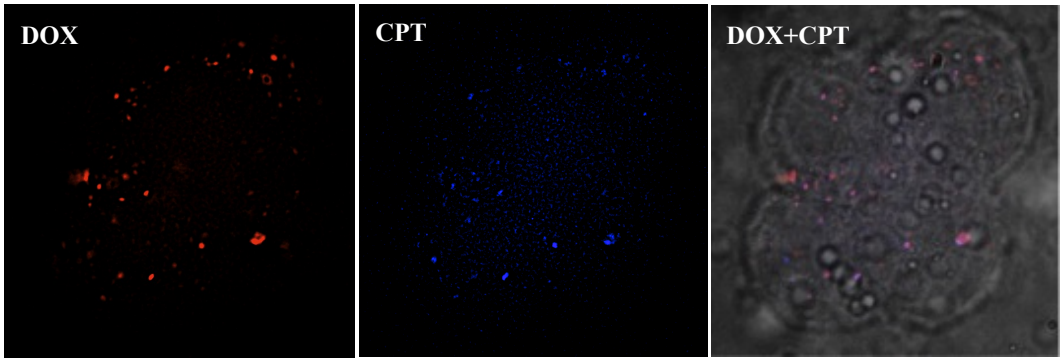


Fig. 2.5. Cellular colocalization studies of the DOX-PLA and CPT-PLA loaded dual-drug nanoparticles. Fluorescence microscopy images showing the colocalization of DOX and CPT in the cellular compartment of MDA-MB-435 breast cancer cells.

2.3.5 *In Vitro* Cytotoxicity of Dual-Drug Nanoparticles

After having confirmed that the nanoparticles contain a mixture of DOX and CPT, we next examined the cytotoxicity of these dual-drug loaded nanoparticles in comparison to the cocktail mixtures of the corresponding single-drug loaded nanoparticles against MDA-MB-435 breast cancer cells in vitro. The cocktail system was prepared by mixing DOX-PLA loaded nanoparticles and CPT-PLA loaded nanoparticles at a ratio that is equivalent to the DOX-PLA:CPT-PLA molar ratio in the dual-drug nanoparticles. Figure 2.6 shows the results of IC50 measurements of the dual-drug loaded nanoparticles and cocktail combination of single-drug loaded nanoparticles. It was found that the dual-drug loaded nanoparticles consistently showed higher potency as compared to the cocktail systems for the 3 different drug ratios. In the 3:1, 1:1, and 1:3 DOX-PLA:CPT-PLA combinations, the dual-drug loaded nanoparticles showed an enhancement in efficacy by 3.5, 2.5, and 1.1 times, respectively, compared to the cocktail particle mixtures. This enhanced cytotoxicity of the dual-drug delivery system can be explained, at least partially, by the fact that dual-drug loaded nanoparticles can deliver more consistent combination drug payloads when compared to cocktail nanoparticle systems and hence maximize their combinatorial effect. In the cocktail variations in the nanoparticle uptake and the random drug distribution in cells likely compromised the efficacy of the drug combinations. Figure 2.5 suggests that the dual-drug loaded nanoparticles enable concurrent combination drug delivery through particle endocytosis. Once engulfed by the plasma membrane, nanoparticles are transported by endosomal vesicles before

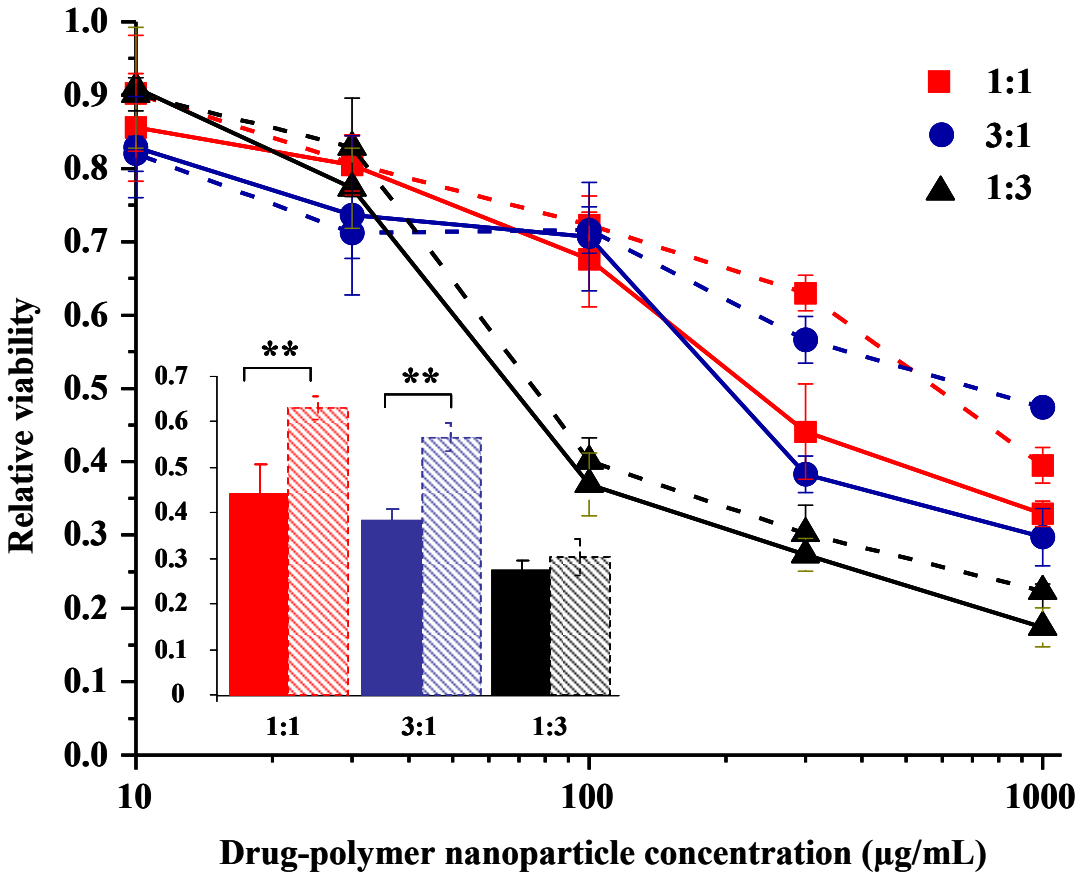


Fig. 2.6. A comparative study of cellular cytotoxicity of the DOX-PLA and CPT-PLA loaded dual-drug nanoparticles against the MDA-MB-435 breast cancer cells. The ratios shown in figure legends are the molar ratios of DOX-PLA to CPT-PLA. Solid lines represent the dual-drug loaded nanoparticles and dashed lines represent the cocktail mixture of DOX-PLA loaded and CPT-PLA loaded single-drug nanoparticles. All samples were incubated with cells for 24 h, and the cells were subsequently washed and incubated in media for a total of 72 h prior to MTT assay (n=4). Inset shows the cytotoxicity comparison of combinatorial and cocktail nanoparticle combination at 300 µg/mL nanoparticle concentration, A paired t-test was performed (**p<0.01, n=4).

unloading their drug payloads. This endocytic uptake mechanism is particularly favorable to the drug-polymer conjugate system used in the present combinatorial drug delivery scheme. The pH drop associated with endosome maturation subjects the nanoparticles to an acidic environment and enzymatic digestions (104, 105), which facilitate the cleavage of the ester linkage between the drug and the polymers. In addition, the degradation of the polymer PLA releases lactic acid to further lower the pH surrounding the nanoparticles, thereby further accelerating the drug release.

2.4 Conclusions

In conclusion, a new and robust approach for combination chemotherapy was presented by incorporating two different types of drugs with ratiometric control over drug loading into a single polymeric nanoparticle. By adapting metal alkoxide chemistry, drug conjugated polymers were synthesized in a quantitative yield with 100% monomer conversion, resulting in the formation of highly hydrophobic drug-polymer conjugates. These drug-polymer conjugates were successfully encapsulated into lipid-coated polymeric nanoparticles with over 90% loading efficiency. Using DOX and CPT as two model chemotherapy drugs, various ratios of DOX-PLA and CPT-PLA were loaded into the nanoparticles, yielding particles that are uniform in size, size distribution and surface charge. The cytotoxicity of these dual-drug carrying nanoparticles was compared with their cocktail their cocktail mixtures of single-drug

loaded nanoparticles and showed superior therapeutic effect. This strategy can also be exploited for various other chemotherapeutic agents containing hydroxyl groups as well as different types of combinations for combinatorial treatments of various diseases. While only two drugs (DOX and CPT) were used to demonstrate the concept of this combinatorial drug delivery approach, this method can be generalized to incorporate three or more different types of drugs into the same nanoparticles with ratiometro control over drug loading.

Chapter 2, in full, is a reprint of the material as it appears in Molecular Pharmaceutics, 2011, Che-Ming Hu, Santosh Aryal, and Liangfang Zhang. The dissertation author was the primary investigator and co-author of this paper.

3. Half-antibody Functionalized Nanoparticles for Targeted Drug Delivery

3.1 Introduction

Pancreatic cancer is the 4th leading cause of cancer-related death in the United States (106). Because of its elusive symptoms, pancreatic cancer patients are often diagnosed at an advanced stage, at which time the tumors are often unresectable and best addressed with chemotherapy. However, most chemotherapeutic regimens show little to no response against pancreatic cancer. Even the current first-line drug, gemcitabine, shows only modest improvement in patient survival (107). A recent study by Olive et al. suggests that low efficacy of chemotherapy against pancreatic cancer is due to the poor vascularization and inadequate drug perfusion at the tumoral sites (108). Such a clinical challenge calls for new and more effective drug delivery strategies that can enhance the drug availability at the tumor sites.

To address this fundamental issue in pancreatic cancer treatment, here we propose a targeted drug delivery platform consisting of a lipid-polymer hybrid nanoparticle (NP) to carry therapeutic payloads and a selectively reduced anti-CEA half-antibody (hAb) to target pancreatic cancer cells. It is hypothesized that the targeted NPs can preferentially bind to pancreatic cancer cells rather than normal cells. Given the high drug loading capacity of each lipid-polymer hybrid NP, the cancer cells are expected to be destroyed even though only few NPs are taken up by one cell.

The lipid-polymer hybrid NPs consist of a biodegradable and biocompartible hydrophobic polymeric core made of poly $_{D,L}$-lactic-co-glycolic acid (PLGA), a monolayer of phospholipids, and an outer corona layer made of polyethylene glycol (PEG). Despite their complex structure, these hybrid NPs are synthesized in a simple, single-step fashion, which allows future scale-up production and cost-effective real-life applications (109). Several features make these NPs a promising drug delivery platform, including biocompatibility, biodegradability, sustained drug-release profiles, functionalizable surface, excellent stability in blood, and most importantly, high drug loading yield (102). These properties provide a basis for a stable, high-payload targeted drug delivery vehicle that can potentially maximize the chemotherapeutic efficacy against target cancer cells. ,

For the targeting ligand, we selected anti-CEA monoclonal antibody (mAb) as a basis because CEA is overexpressed in 90% of pancreatic tumors (110). In a study of using fluorophore-conjugated anti-CEA mAb for pancreatic cancer visualization, Kaushal et al. demonstrated that the mAb could effectively and safely deliver

fluorescent dyes to subcutaneous, orthotopic, and metastatic human pancreatic cancer xenografts in nude mice (111). Several reports have also conjugated anti-CEA mAb with NPs for various applications (112-114). In the case of NP drug delivery, however, whole antibodies have several limitations. For instance, the large hydrodynamic size of antibodies significantly increases nonspecific uptake by the reticuloendothelial system (RES) and reduces the NP circulation half-life (115). In addition, the nonspecific nature of antibody conjugation with NPs, typically involving random carboxyl-amine reaction, could result in hindered binding sites of the antibody and particle dimerization. Smaller antibody variants, such as single-chain variable fragments (svFc) (116) diabodies, and minibodies (117, 118) have emerged in research settings to address these issues. Here we selectively reduced the disulfide bonds between the heavy chains of the anti-CEA mAb using low molar excess of reducing agent to produce anti-CEA half-antibodies (hAb). The resulting hAb possess intact binding sites and reactive thiol groups on their constant region. These hAb retain their targeting ability but are smaller in size and can be conjugated in a site-specific manner. Several reports have employed the hAb strategy to deliver imaging agents such as quantum dots and iron oxide (119, 120). To the best of our knowledge, this is the first report that optimizes such a strategy for high-dose targeted drug delivery.

In this study, we successfully synthesized and characterized anti-CEA hAb conjugated lipid-polymer hybrid NPs (Fig. 3.1). We demonstrated the integrity and stability of the complex structure of the targeted NPs after being internalized by the

target cells as well as their targeting specificity toward CEA-presenting pancreatic cancer cells *in vitro*. In addition, using paclitaxel as a model chemotherapy drug, we showed superior cytotoxicity of the targeted NPs against pancreatic cancer cells in comparison with their non-targeted counterparts. A schematic illustration of the targeted NP is shown in figure 3.1.

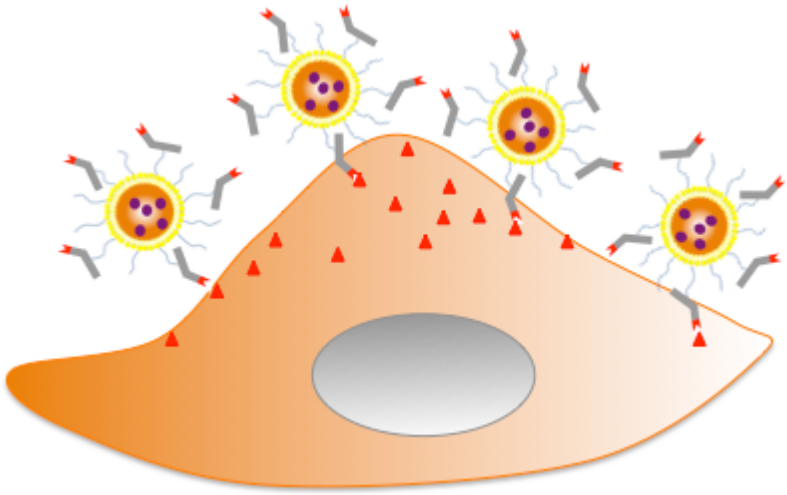


Fig. 3.1. Schematic illustration of hAb functionalized NPs targeting tumor cells through surface antigens.

3.2 Experimental Methods

3.2.1 Conjugation of Fluorophore to Anti-CEA Antibody and PLGA Polymer

Monoclonal antibody specific for CEA was acquired from Biodesign International (Saco ME). The antibody was labeled with Alexa Fluor 488 (Molecular Probes, Eugene, OR) fluorophores following a protocol provided by the manufacturer. Briefly, the monoclonal antibody was reconstituted at 2 mg/mL in 0.1M sodium bicarbonate. 500 uL of the antibody solution were added to the reactive dye and allowed to incubate for 1 hr at room temperature. The antibody-dye conjugates were separated from unconjugated free dyes via a purification column. Alexa Fluor 647 (Molecular Probes, Eugene, OR) was conjugated to carboxy-terminated PLGA polymer through activation by 1-ethyl-3-(3-dimethylaminopropyl) carbodiimide (EDC) and *N*-hydroxysuccinimide (NHS). Briefly, 40 mg of 0.16 dL/g PLGA (Durect Corp, Cuppertino, CA) dissolved in 1.6 mL of dimethylformamide (DMF) were mixed with 40 mg of EDC and 20 mg of NHS (Pierce, Rockford, IL) for 15 min. The 534 μL of 0.5 mg/mL Alexa Fluor 647 solutions were added to the mixture and incubated overnight. The unconjugated dyes were removed by cold methanol wash. The fluorophore-conjugated PLGA was then vacuumed dried and re-dissolved in acetonitrile.

3.2.2 Synthesis and Characterization of Anti-CEA hAb Targeted Lipid-polymer Hybrid NPs

Lipid-polymer hybrid NPs were prepared via self-assembly of PLGA (Lactel, Pelham, AL), lecithin (soybean, refined, molecular weight: ~330 Da; Alfa Aesar,

Ward Hill, MA), carboxyl-terminated DSPE-PEG (1,2-distearoyl-sn-glycero-3-phosphoethanolamine- N-carboxy (polyethylene glycol)2000) and maleimide-terminated DSPE-PEG (Avanti Polar Lipids, Alabaster, AL) through a single-step nanoprecipitation method following a previously published protocol.[4] Briefly, 0.12 mg of lecithin and 0.26 mg of DSPE-PEG (the molar ratio between DSPE-PEG-COOH and DSPE-PEG-maleimide is determined by the amount of anti-CEA hAb to be conjugated to the NP surface) were dissolved in 2 mL 4 wt% ethanol aqeous solution. In parallel, 1 mg of PLGA polymer was dissolved in 1 mL acetonitrile. The resulting PLGA solution was then added into the lipid solution dropwise under gentle stirring. The mixed solution was vortexed vigorously for 3 minutes followed by gentle stirring for 2 hours at room temperature. The remaining organic solvent and free molecules were removed by washing the NP solution three times using an Amicon Ultra-4 centrifugal filter (Millipore, Billerica, MA) with a molecular weight cut-off of 10 kDa. The NPs with maleimide moieties were then incubated with selectively reduced anti-CEA hAb for 4 hrs. Finally, the unconjugated antibodies were removed by centrifugation using 300 kDa Pall Nanosep® centrifugal device (Sigma-Aldrich, St. Louis, MO).

The cleaved antibodies were separated on a SDS-PAGE 3-8% Tri-Acetate 10-well mini gel in tri-acetate running buffer using NovexSureLockXcell Electrophoresis System (Invitrogen). The samples were run at 150V for 1 hr and the resulting polyacrylamide gel was stained in SimplyBlue™ (Invitrogen) overnight for visualization. To quantify the ligand conjugation, Alexa Fluor 488 fluorescence in the

hAb-NP solution was measured and matched to a standardization curve. The resulting hAb content was converted to mole. The number of NPs per 1mg of PLGA was approximated under the assumptions of spherical structure and uniform polymer density. Mass of each NP was estimated based on a particle diameter of 83 nm and a PLGA density of 1.2 g/mL. Assuming no loss in PLGA, the number of NPs was derived by dividing 1mg by the mass of a single NP.

NP size (diameter, nm) and surface charge (zeta potential, mV) were measured by dynamic light scattering (DLS) using Nano-ZS, Model ZEN3600 (Malvern, UK). NPs (~500 μg) were dispersed in water (~1 mL) and measurements were performed in triplicates at room temperature. The morphology and particle size were further characterized using scanning electron microscopy (SEM). Samples for SEM were prepared by dropping 5 μL of NPs solutions onto a polished silicon wafer. After drying the droplet at room temperature overnight, the sample was coated with chromium and then imaged by SEM.

3.2.3 Cellular Targeting and Internalization Studies

The human pancreatic cell lines BxPC-3 and XPA-3 were maintained in RPMI (Gibco-BRL, Grand Island, NY) supplemented with 10% fetal calf albumin (FCS; Hyclone, Logan, UT), penicillin/streptomycin (Gibco-BRL), L-glutamine (Gibco-BRL), MEM nonessential amino acids (Gibco-BRL), sodium bicarbonate (Cellgro, Herndon, VA), and sodium pyruvate (Gibco-BRL). Both cell lines were

cultured at 37°C with 5% CO_2 and were plated in chamber slides (Cab-Tek II, eight wells; Nunc, Rochester, NY) with the aforementioned media. On the day of the experiment, cells were washed with pre-warmed PBS and incubated with pre-warmed RPMI media for 30 min before adding 100 μg of hAb-NPs or non-targeted NPs with the same amount of Alexa Fluor 647 dyes. The NPs were incubated with cells for 30 min at 37°C, washed with PBS 3 times, fixed with tissue fixative (Millipore, Bellerica, MA) for 30 min at room temperature, stained with 4',6-diamidino-2-phenylindole (DAPI, nucleus staining), mounted in ProLong® Gold antifade reagent (Invitrogen), and imaged using deconvolution scanning fluorescence microscopy (DeltaVision System, Applied Precision, Issaquah, WA). Digital images of blue, green, and red fluorescence were acquired using a 40x and a 100x oil immersion objective and DAPI, FITC, and CY5 filters, respectively. Images were overlaid and deconvoluted using softWoRx software.

3.2.4 *In vitro* Cytotoxicity Study

To prepare drug-encapsulated NPs, 0.1 mg of paclitaxel (Sigma-Aldrich, St Louis, MO) was dissolved into the 1 mg of PLGA acetonitrile solution before the nanoprecipitation process. To quantify the loading yield of paclitaxel, the paclitaxel-loaded NPs were dissolved in a 70% acetonitrile aqueous solution and left on a vortex at room temperature for two days. Paclitaxel was quantified by high performance liquid chromatography (HPLC). The column used was μBONDAPAK 4.6x150 mm.

The paclitaxel absorbance was measured by a UV/Vis detector at 230 nm in an acetonitrile/water gradient mobile phase (1 mL/min). The mobile phase acetonitrile/water ratio started at 50/50 at 0 min and increased to 100% acetonitrile over 10 min. Acetonitrile was then held for 4 min before returning to a 50/50 ratio in 14-25 min. Each set of data was measured with a calibration curve. For the cytotoxicity study, BxPC-3 cells were grown in 96-well plates at concentrations leading to 60% confluence in 24 h (40000 cell/cm^2). NPs with different paclitaxel loading were incubated with the cells in RPMI for 1 hr. Then the cells were washed and supplemented with fresh media. Following 72 hrs of culture, cell viability was assessed with the ATPLite 1-step luminescence ATP detection assay (PerkinElmer, Waltham, MA) following a protocol provided by the manufacturer.

3.3 Results and Discussions

Figure 3.2 illustrates the synthesis scheme of anti-CEA hAb conjugated lipid-polymer hybrid NPs. Briefly, the maleimide-terminated hybrid NPs were self-assembled from their building blocks via a nanoprecipitation method following a previously described protocol.(109) Tris (2-carboxyethyl) phosphine (TCEP) with a molar excess of 3x over the molar concentration of the anti-CEA mAb was used to

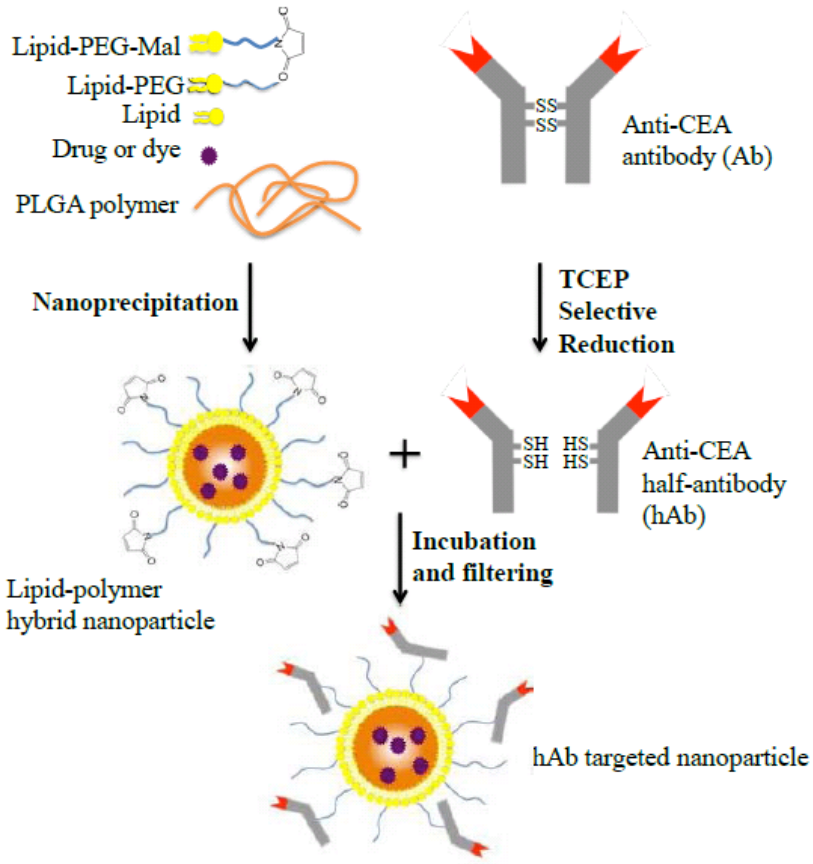


Fig. 3.2. Schematic diagram of the synthesis of anti-CEA half-antibody (hAb) conjugated lipid-polymer hybrid NPs.

selectively reduce the mAb into anti-CEA hAb. Subsequentially, the hAb were conjugated with the hybrid NPs through maleimide-thiol coupling. The resulting hAb-NPs were then filtered to remove excess antibodies (both uncleaved mAb and excess hAb) before further characterization and application.

3.3.1 Synthesis of Anti-CEA hAb

Since the extent of antibody reduction governs the conjugation efficiency as well as the targeting ability, the selective reduction process was optimized using sodium dodecyl sulfate polyacrylamide gel electrophoresis (SDS-PAGE). To confirm the production of hAb and to optimize the selective reduction process, anti-CEA mAb were mixed with different molar excess of TCEP for 4 hrs and then separated and visualized. Figure 3.3A showed the SDS-PAGE results of reduced anti-CEA mAb under various molar excess of TCEP. Using the reference molecular weight ladder, the whole mAb (~130kDa) and three distinct cleavage products - hAb (~67kDa), heavy-chain fragments (~46kDa), and light-chain fragments (~21kDa) - were clearly identified. The presence of four distinct bands suggests that the disulfide bonds between the two heavy-chains were preferentially cleaved resulting in the formation of hAb. If all disulfide bonds in the mAb had been cleaved equally, two additional bands would have been observed, corresponding to double-heavy-chain fragments (~92kDa) and single-light-chain-double-heavy-chain fragments (~113kDa). Figure

3.3A also revealed the extent of mAb cleavage under different TCEP concentrations. It was observed that under 30x molar excess of TCEP the mAb were completely cleaved to heavy-chain and light-chain fragments. These fragments showed no binding affinity toward CEA-presenting pancreatic cancer cells (data not shown). We found that 3x molar excess of TCEP would maximize the yield of hAb and minimize the production of non-targeting fragments that compete with hAb for maleimide conjugation sites on the hybrid NP surface.

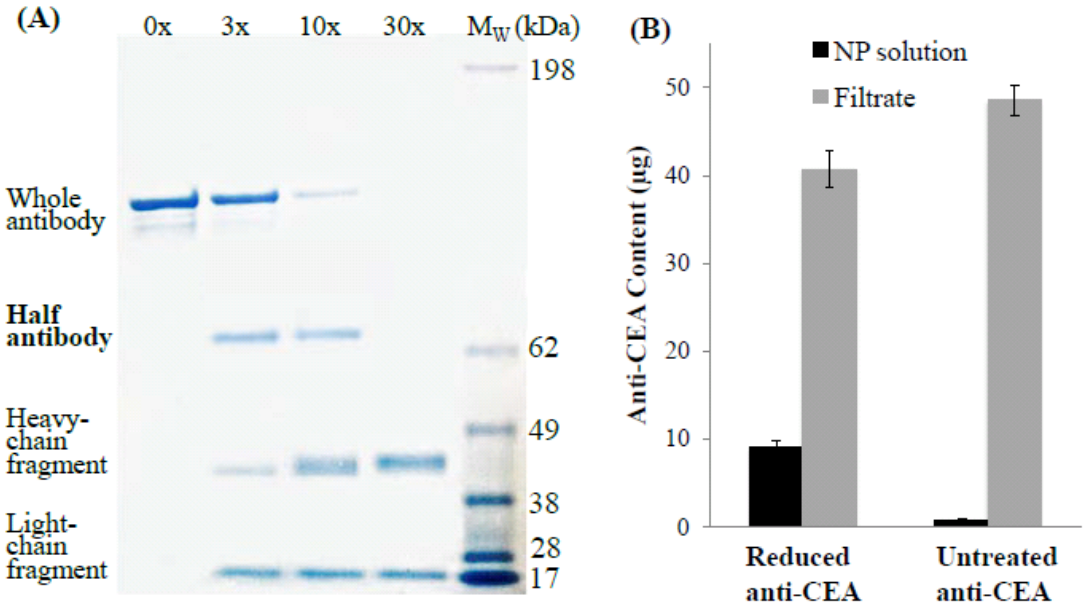


Fig. 3.3. (A) Gel electrophoresis results of anti-CEA antibody reduction at TCEP (reducing agent) concentration of 0x, 3x, 10x and 30x over the concentration of the antibody, respectively. The rightmost lane represents a standard molecular weight ladder. (B) Quantifying the conjugation yield of 1 mg of maleimide-terminated hybrid NPs with 50 µg of anti-CEA antibody reduced by 3x TCEP versus 50 µg of untreated anti-CEA antibody.

3.3.2 Synthesis and Characterization of hAb-NP conjugates

The resulting hAb was conjugated to the hybrid NPs through maleimide-thiol coupling and the reaction was confirmed and quantified using fluorescence measurements (Figure 3.3B). Before TCEP reduction, anti-CEA mAb were covalently labeled with Alex-488 fluorophores. In the study, 50 μg of reduced anti-CEA mAb (3x molar excess of TCEP) were incubated with 1 mg of maleimide-terminated hybrid NPs (molar ratio: mAb/NP ≈ 150/1) for 4 hrs before the solution was filtered through a membrane with a molecular weight cutoff of 300 kDa. Fluorescence readings of the NP solution and the corresponding filtrate indicate that approximately 9.7 μg (or 19.4%) of selectively reduced anti-CEA mAb were conjugated to 1 mg of NPs, which translates to a 32:1 ligand-to-particle molar ratio (see experimental section for this estimation). To confirm that the retained fluorescence was due to maleimide-thiol conjugation rather than non-specific absorption of uncleaved anti-CEA mAb, noting that intact mAb do not react with the maleimide-terminated NPs, the NP solution was then mixed with 50 μg of untreated anti-CEA mAb. It was found that less than 1% (0.47 μg) of the mAb was retained in the NP solution. This control experiment suggests that the filter membrane used in this study was sufficient enough to remove all free mAb or their fragments from the NP solution and negligible amount of mAb non-specifically absorbs onto the NP surface.

The NP diameter and surface zeta potential in water were compared before and after the hAb conjugation using dynamic light scattering (DLS). The results

showed a slight increase in particle size (83 nm to 95 nm) and a less negative zeta potential (-61 mV to -55 mV) following the hAb conjugation (Figure 3.4A). The size increase corresponds to the coating of the hAb around the NP surface. The increase in zeta potential, on the other hand, is likely due to the shielding of the negatively charged NP surface by the nearly neutral anti-CEA hAb moieties. Scanning electron microscopy (SEM) images (Figure 3.4B) of the hAb-conjugated hybrid NPs revealed their spherical structures with an averaged diameter of sub-100 nm, which was consistent with the DLS results.

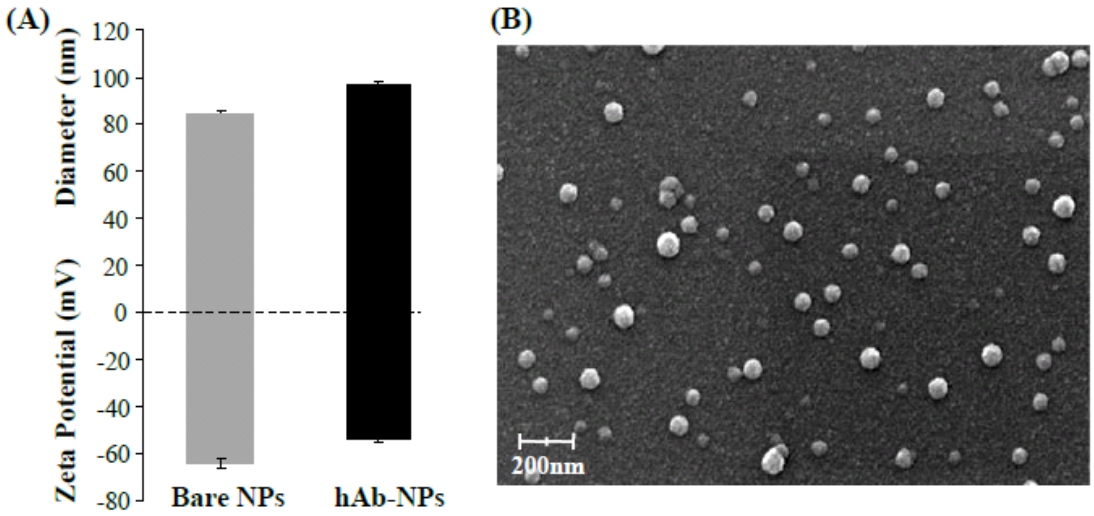


Fig. 3.4. (A) Size and surface zeta potential of the hybrid NPs before and after hAb conjugation determined by dynamic light scattering. (B) SEM image of hAb targeted lipid-polymer hybrid NPs.

3.3.3 Targeting Ability of hAb-NPs

After having synthesized the hAb-NPs and characterized their physicochemical properties, we next examined their targeting ability, particularly against CEA-presenting pancreatic cancer cells. We began by confirming the concurrent delivery of the lipid shell and the PLGA core of the targeted NPs using a dual-fluorophore system. One concern of using the lipid-polymer hybrid NPs stems from the integrity of their core-shell structure, especially when the shell is conjugated with targeting moieties. That is, the hAb conjugated lipid shell may detach from the PLGA core during the delivery process, therefore the hAb cannot target the drug loaded PLGA core to the sites of action. To test this possibility, the anti-CEA hAb and the PLGA core were labeled with Alexa-488 (green) and Alexa-647 (red), respectively. Targeted NPs simultaneously containing these two dyes were incubated with CEA-presenting human pancreatic adenocarcinoma cells (BxPC-3) and subsequently imaged using deconvolution scanning fluorescence microscopy. The matching overlay of the green and red fluorescence (Fig. 3.5A-C) from the same NPs at corresponding excitation wavelengths suggests that neither the lipid shell nor the targeting hAb ligands was striped from the polymeric core following cell binding and particle internalization.

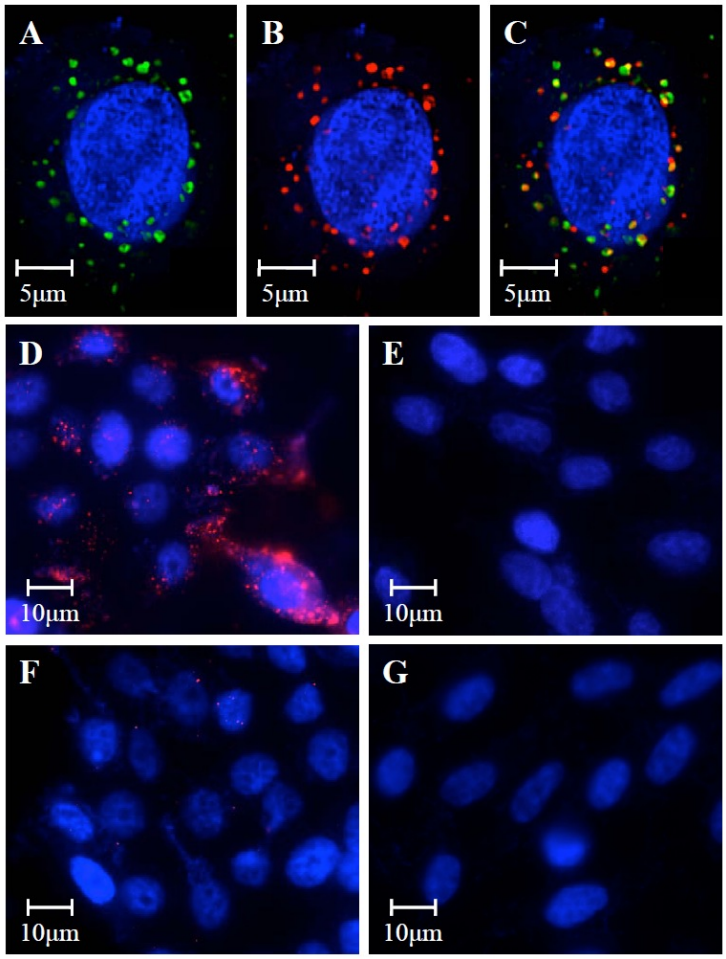


Fig. 3.5. Scanning fluorescence microscopy images demonstrated the co-delivery of (A) the lipid shell to which the hAb conjugated (visualized with green Alexa Fluor 488 dyes) and (B) the PLGA polymeric core (visualized with red Alexa Fluor 647 dyes) to CEA-positive BxPC-3 cells (nucleus stained in blue with DAPI). (C) The overlay of the green and red fluorescence confirmed the integrity of the lipid-polymer hybrid NP structure after being internalized by the target cells. Targeting specificity was confirmed by incubating (D) CEA-positive BxPC-3 cells with anti-CEA hAb targeted NPs, (E) CEA-negative XPA-3 cells with anti-CEA hAb targeted NPs, (F) CEA-positive BxPC-3 cells with non-targeted NPs, and (G) CEA-negative XPA-3 cells with non-targeted NPs.

The targeting specificity of the hAb-NPs was evaluated by incubating BxPC-3 and a non-CEA-presenting human pancreatic cancer cell line (XPA-3) with hAb-NPs and non-targeted hybrid NPs without hAb conjugation. As shown in Figure 3.5D-G, the hAb-NPs effectively bound to the CEA positive BxPC-3 cells (Fig. 3.5D) but remained stealthy to the CEA negative XPA-3 cells (Fig. 3.5E). In contrast, the non-targeted hybrid NPs showed negligible cellular uptake by either BxPC-3 cells (Fig. 3.5F) or XPA-3 cells (Fig. 3.5G). This selective targeting could only be attributed to the complementary binding to the carcinoembryonic antigens by the anti-CEA hAb. Such a mechanism could enhance the cancer cell killing effect through receptor-mediated endocytosis which facilitates particle internalization (121, 122). After a single hAb-NP was taken up by a target cell, it may release enough drug payloads to show therapeutic activity.

3.3.4 Cytotoxicity of Paclitaxel-loaded hAb-NPs

To examine the *in vitro* cellular cytotoxicity of the anti-CEA hAb targeted NPs against pancreatic cancer cells, we chose paclitaxel as a model hydrophobic chemotherapy drug. Paclitaxel is a widely used anticancer drug and has shown great therapeutic efficacy against pancreatic cancer (123). An additional reason of choosing paclitaxel is that the drug can be readily loaded into the hydrophobic PLGA core of the hybrid NPs with high and controllable loading yields. In the study, hAb-NPs with various paclitaxel loading yields were incubated with BxPC-3 cells. The resulting cellular cytotoxicity was measured by an ATP cellular viability assay and was

normalized to that of BxPC-3 cells treated by PBS buffer. Non-targeted hybrid NPs with the corresponding paclitaxel loading yields were used in parallel as a control. The actual paclitaxel loading of different NP formulations were quantified using high performance liquid chromatography (HPLC) following a published protocol.(92) The results showed that paclitaxel loading yield can be precisely tuned by varying the initial drug input during NP preparation process (Fig. 3.6 inset). Here up to ~38 μg of paclitaxel were encapsulated into 1 mg of the hybrid NP for the cytotoxicity study. This 3.8 wt% drug loading yield can be converted to roughly 10,000 paclitaxel drug molecules per NP, calculating from the diameter of the NP (83 nm), PLGA density (1.2 g/mL) and the molecular weight of paclitaxel (854 Da). Speculatively, a few drug-loaded NPs taken up by one cancer cell may be able to provide a sufficiently high dose of paclitaxel that can kill the cancer cell. It is worth noticing that the loading yield of paclitaxel can be further improved by tuning the formulation parameters of the hybrid NPs but this is beyond the focus of this study.

After the paclitaxel-loaded hybrid NPs (both targeted and non-targeted) were prepared, the BxPC3 cells were incubated with the NPs loaded with different doses of paclitaxel for 1 hr. Then the excess NPs were washed in PBS buffer and the cells were cultured in fresh media for up to 72 hrs before they were subject to ATP assay. The luminescence signals of all samples were normalized to that of the cells in the absence of NPs to calculate the relative cellular viability of each circumstance. The results showed that the hAb targeted NPs had enhanced cytotoxicitiy at all levels of paclitaxel dosage, especially at 359 nM (Fig. 3.6), where the targeted NPs and non-

targeted NPs resulted in 25.7±7.2% and 58.7±9.9% relative cellular viability, respectively. ANOVA test showed that the difference in relative viability of the targeted and non-targeted NPs was significant at both 359 nM and 984 nM ($p<0.01$) of paclitaxel loading. An IC50 of 251 nM and 526 nM were obtained for the hAb-NPs and non-targeted NPs, respectively, which translated to a more than 2-fold increase in therapeutic efficacy due to the anti-CEA hAb targeting. It needs to be noted that without drug loading, neither the targeted NPs nor the non-targeted NPs showed any

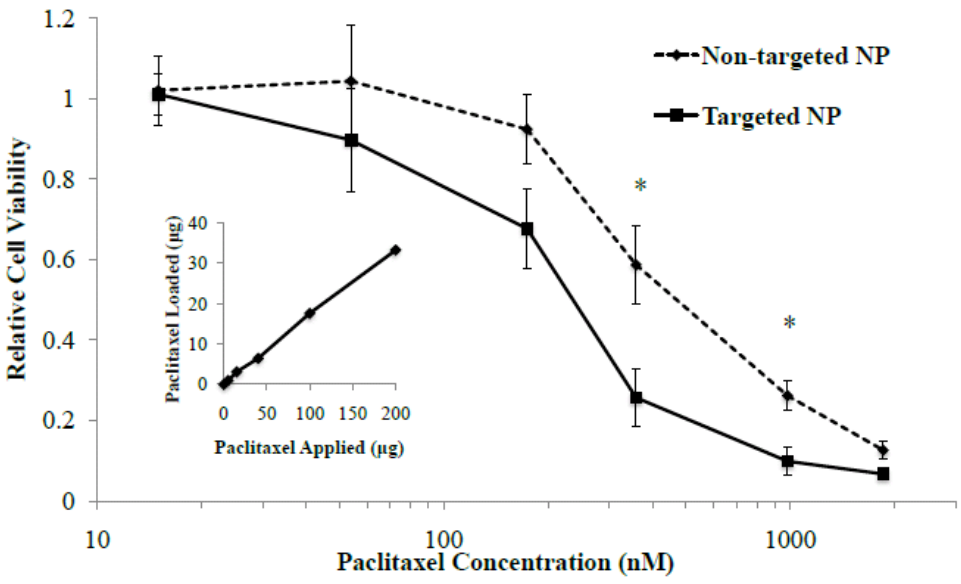


Fig. 3.6. Relative viability of BxPC-3 cells incubated paclitaxel-loaded hAb targeted NPs (solid line) and non-targeted NPs (dashed line) with various paclitaxel loading yields using ATP assay. The results were normalized to controls without NP treatment. ANOVA test: *$p<0.01$ ($n=8$). Inset: paclitaxel loading vs. paclitaxel applied during NP preparation per 1mg of NPs.

cytotoxicity against the cells. The biocompatibility of these NPs is consistent with previous findings on lipid-polymer hybrid NPs(102). Therefore, the hAb-conjugated NPs can be safely used as a drug delivery vehicle for *in vivo* applications.

3.4 Conclusions

In summary, we have successfully synthesized a targeted NP drug delivery platform specific to pancreatic cancer cells using FDA-approved biomaterials and selectively reduced anti-CEA half-antibodies. Ligand-to-particle molar ratio, particle size, surface charge, and drug loading yield have been characterized and could be controlled for specific therapeutic applications. In addition, we have demonstrated the targeting specificity of the synthesized targeted NPs as well as their enhanced cellular cytotoxicity against target cells compared to their non-targeted counterparts. This platform has great therapeutic potentials as it can effectively deliver a variety of chemotherapeutic drugs to pancreatic tumors in a targeted manner. Additional *in vivo* studies are required to examine the pharmacokinetics, biodistribution and therapeutic efficacy of the hAb targeted NPs before further applications can be considered.

Chapter 3, in full, is a reprint of the material as it appears in Molecular Pharmaceutics, 2010, Che-Ming Hu, Sharmeela Kaushal, Hop S. Tran Cao, Santosh Aryal, Marta Sartor, Sadik Esener, Michael Bouvet, and Liangfang Zhang. The dissertation author was the primary investigator and author of this paper.

Chapter 4 Erythrocyte Membrane-camouflaged Polymeric Nanoparticles as a Novel Long-circulating Delivery Platform

4.1 Introduction

Long-circulating polymeric nanoparticles have significant clinical impact as they promise sustained systemic delivery and better targeting through both passive and active mechanisms (124-126). Different approaches including modifications on particle size, surface, shape, and flexibility have been explored to extend particle residence time *in vivo* (127-129). The current gold standard for nanoparticle stealth coating is polyethylene glycol (PEG). The adoption of PEG as a stealth moiety on nanoparticle surface has led to great success with several clinical products (125, 126), but recent observation of anti-PEG immunological response has triggered the interest of further investigation on its biological relevance (75). Synthetic zwitterionic

materials such as poly(carboxybetaine) and poly(sulfobetaine) have been proposed as alternatives to PEG because of their strong hydration that is highly resistant to nonspecific protein adsorption (130, 131). In addition, recent advances in molecular and cellular biology have inspired scientists and nanotechnologists to model nanocarriers after red blood cells (RBCs), which are nature's long-circulating delivery vehicles. Properties of RBCs such as their structure and surface proteins have been taken as design cues to devise the next-generation delivery platforms (132-134).

While significant efforts have been devoted to bridging the gap between synthetic nanomaterials and biological entities, an RBC-mimicking delivery vehicle has remained elusive to biomedical researchers. One major challenge lies in the difficulty in functionalizing nanoparticles with the complex surface chemistry of a biological cell. Despite the recent great progress in reducing macrophage engulfment of polystyrene beads following their conjugation with an immunosuppressive RBC membrane protein, CD47 (133), current chemistry-based bioconjugation techniques often lead to protein denaturation. In addition, these bottom-up approaches are largely inadequate in duplicating a complex protein makeup on a nanoscale substrate. Inspired by the concept of bridging synthetic and natural materials and by the need to reinvent nanoparticle functionalization, we herein develop an RBC membrane-camouflaged polymeric nanoparticle platform through a top-down method. By extruding poly(lactic-co-glycolic acid) (PLGA) particles with preformed RBC membrane-derived vesicles, we coat the sub-100nm polymeric particles with the

bilayered RBC membranes including both lipids and the corresponding surface proteins (Fig. 4.1). This approach aims to camouflage the nanoparticle surface with the erythrocyte exterior for long circulation while retaining the applicability of the polymeric core. We report the physical characterizations, physicochemical properties, protein contents, pharmacokinetics, and biodistributions of this biomimetic nanoparticle delivery platform.

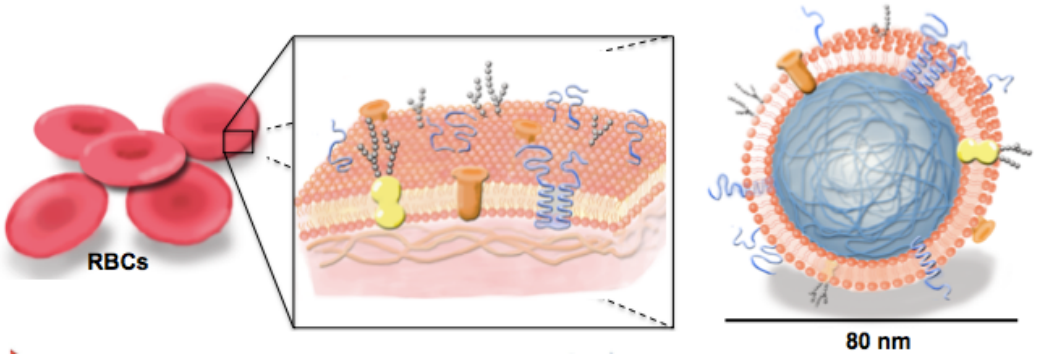


Fig. 4.1. Schematic illustration of RBC membrane camouflaged PLGA NPs.

4.2 Materials and Methods

4.2.1 Red Blood Cell Ghost Derivation

RBC ghosts devoid of cytoplasmic contents were prepared following previously published protocols with modifications (135). Whole blood was first

withdrawn from male ICR mice (6-8wks) obtained from Charles River Laboratories (Wilmington, MA) through cardiac puncture using a syringe containing a drop of heparin solution (Cole-Parmer, Vernon Hills, IL). The whole blood was then centrifuged at 2000 rpm for 5 minutes at 4°C, following which the serum and the buffy coat were carefully removed. The resulting packed RBCs were washed in ice cold 1X PBS prior to hypotonic medium treatment for hemolysis. The washed RBCs were suspended in 0.25X PBS in an ice bath for 20 minutes and were centrifuged at 2000 rpm for 5 minutes. The hemoglobin was removed whereas the pink pellet was collected. The resulting RBC ghosts were verified using phase contrast microscopy, which revealed an intact cellular structure with an altered cellular content.

4.2.2 Preparation of RBC Membrane-derived Vesicles

The collected RBC ghosts were sonicated in a capped glass vial for 5 minutes using a FS30D bath sonicator (Fisher Scientific, Pittsburgh, PA) at a frequency of 42 kHz and power of 100W. The resulting vesicles were subsequently extruded serially through 400 nm and then 100 nm polycarbonate porous membranes using an Avanti mini extruder (Avanti Polar Lipids, Alabaster, AL). To visualize the liposomal compartment in the RBC membrane-derived vesicles, 1mL of whole blood was mixed with 20 ug of 1,2-Dimyristoyl-sn-Glycero-3-Phosphoethanolamine-N-(Lissamine Rhodamine B Sulfonyl) (Ammonium Salt) (DMPE-RhB) (Avanti Polar Lipids, Alabaster, AL) during the vesicle preparation process. The size of the RBC

membrane-derived vesicles was measured by dynamic light scattering (DLS) after each preparation step.

4.2.3 Preparation of PLGA Nanoparticles

The PLGA polymeric cores were prepared using 0.67dL/g carboxy-terminated 50:50 poly($_{DL}$-lactide-co-glycolide) (LACTEL Absorbable Polymers, Cupertino, CA) in a solvent displacement process. The PLGA polymer was first dissolved in acetone at a 1 mg/mL concentration. To make 1 mg of PLGA nanoparticles, 1 mL of the solution was added dropwise to 3 mL of water. The mixture was then stirred in open air for 2 hours. The resulting nanoparticle solution was filtered with 10K MWCO Amicon Ultra-4 Centrifugal Filters (Millipore, Billerica, MA) and resuspended in 1 mL PBS (1X, pH=7.4). For fluorescence microscopy imaging and *in vivo* particle tracking purposes, 2μg of 1,1'-dioctadecyl-3,3,3',3'-tetramethylindodicarbocyanine, 4-chlorobenzenesulfonate salt (DiD) dye (Invitrogen, Carlsbad, CA) were added to the PLGA acetone solution prior to PLGA nanoparticle synthesis. The release of DiD dye from PLGA nanoparticles was examined using a dialysis method in which 100 μL of the prepared nanoparticle solutions were loaded into a Slide-A-Lyzer MINI dialysis microtube with a molecular weight cutoff of 3.5 kDa (Pierce, Rockford, IL). The nanoparticles were dialyzed in PBS buffer at 37 °C. The PBS solution was changed every 12 hours during the dialysis process. At each predetermined time point, nanoparticle solutions from three mini dialysis units were collected separately for dye

quantification using an Infinite M200 multiplate reader (TeCan, Switzerland). As a control particle, the PEG-coated lipid-PLGA hybrid nanoparticles were prepared through a nanoprecipitation method.

4.2.4 Fusion of RBC Membrane-derived Vesicles with PLGA Nanoparticles

To fuse the RBC membrane-derived vesicles with the PLGA nanoparticles, 1 mg of PLGA nanoparticles was mixed with RBC membrane-derived vesicles prepared from 1 mL of whole blood and then extruded 7 times through a 100 nm polycarbonate porous membrane using an Avanti mini extruder. The mixture ratio was estimated based on the membrane volume of RBCs and the total membrane volume required to fully coat 1 mg of PLGA nanoparticles. Parameters used for the estimation include mean surface area of mouse RBCs ($75\mu m^2$) (136), membrane thickness of RBC (7nm), density of 50:50 PLGA nanoparticles ($1.34g/cm^3$) (137), red blood cell concentration in mouse blood (7 billion per mL) (138), and the mean particle size as measured by DLS before and after the RBC membrane coating. An excess of blood was used to compensate for the membrane loss during RBC ghost derivation and extrusion. The resulting RBC membrane-coated PLGA nanoparticles were dialyzed against 30 nm porous membranes (Avanti Polar Lipids) for 24 hours and concentrated through nitrogen purging. The particle size and polydispersity remained identical following dialysis and concentration.

4.2.5 Characterization of RBC Membrane-coated PLGA Nanoparticles

Nanoparticle size (diameter, nm), polydispersity, and surface charge (zeta potential, mV) were measured by DLS using Nano-ZS, model ZEN3600 (Malvern, U.K.). Nanoparticles (~500 μg) were suspended in 1X PBS (~1 mL) and measurements were performed in triplicate at room temperature for 2 weeks. Serum stability tests were conducted by suspending the nanoparticles in 100% fetal bovine serum (FBS) (Hyclone, Logan, UT) with a final nanoparticle concentration of 1 mg/mL. The particles were first concentrated to 2 mg/mL and a concentrated 2X FBS was then added at equal volume. Absorbance measurements were conducted using an Infinite M200 multiplate reader. Samples were incubated at 37°C with light shaking prior to each measurement. The absorbance at 560 nm was taken approximately every 30 minutes over a period of 4 hours.

4.2.6 Transmission Electron Microscopy Imaging

The structure of the RBC membrane-coated nanoparticles was examined using a transmission electron microscope. A drop of the nanoparticle solution at a concentration of 4 μg/mL was deposited onto a glow-discharged carbon-coated grid. Five minutes after the sample was deposited the grid was rinsed with 10 drops of distilled water. A drop of 1% uranyl acetate stain was added to the grid. The grid was subsequently dried and visualized using a FEI 200KV Sphera microscope.

4.2.7 Tissue Culture and Nanoparticle Endocytosis

The human epithelial carcinoma cell line (HeLa) was maintained in RPMI (Gibco BRL, Grand Island, NY) supplemented with 10% fetal bovine albumin, penicillin/streptomycin (Gibco-BRL), L-glutamine (Gibco-BRL), MEM nonessential amino acids (Gibco-BRL), sodium bicarbonate (Cellgro, Herndon, VA), and sodium pyruvate (Gibco-BRL). The cells were cultured at 37 °C with 5% CO_2 and were plated in chamber slides (Cab-Tek II, eight wells; Nunc, Rochester, NY) with the aforementioned media. On the day of experiment, cells were washed with pre-warmed PBS and incubated with pre-warmed RPMI media for 30 minutes before adding 100 μg of DMPE-RhB and DiD labeled RBC membrane-coated PLGA nanoparticles. The nanoparticles were incubated with cells for 4 hours at 37 °C. The cells were then washed with PBS 3 times, fixed with tissue fixative (Millipore, Bellerica, MA) for 30 minutes at room temperature, stained with 4′,6-diamidino-2-phenylindole (DAPI, nucleus staining), mounted in ProLong Gold antifade reagent (Invitrogen), and imaged using a deconvolution scanning fluorescence microscope (DeltaVision System, Applied Precision, Issaquah, WA). Digital images of blue, green, and red fluorescence were acquired under DAPI, FITC, and CY5 filters respectively using a 100X oil immersion objective. Images were overlaid and deconvoluted using softWoRx software.

4.2.8 Protein characterization using SDS-PAGE

The RBC ghosts, the RBC membrane-derived vesicles, and the dialyzed RBC membrane coated PLGA nanoparticles were prepared in SDS sample buffer (Invitrogen). The samples were then run on a NuPAGE® Novex 4-12% Bis-Tris 10-well minigel in 3-(N-morpholino) propanesulfonic acid (MOPS) running buffer using NovexSureLockXcell Electrophoresis System (Invitrogen). The samples were run at 150 V for 1 hour, and the resulting polyacrylamide gel was stained in SimplyBlue (Invitrogen) overnight for visualization.

4.2.9 Pharmacokinetics and Biodistribution Studies

All the animal procedures complied with the guidelines of University of California San Diego Institutional Animal Care and Use Committee. The experiments were performed on male ICR mice (6-8 wks) from Charles River Laboratories (Wilmington, MA). To evaluate the circulation half-life of RBC membrane-coated nanoparticles, 150 μL of DiD-loaded nanoparticles were injected into the tail vein of the mice. 20 μL blood was collected at 1, 5, 15, 30 minutes, and 1, 2, 4, 8, 24, 48, and 72 hours following the injection. The same dose of DiD containing PEG-coated lipid-PLGA hybrid nanoparticles and bare PLGA nanoparticles were also tested in parallel as controls. Each particle group contained 6 mice. The collected blood samples were diluted with 30 μL PBS in a 96-well plate before fluorescence measurement. Pharmacokinetics parameters were calculated to fit a two-compartment model.

To study the biodistribution of the nanoparticles in various tissues, 18 mice received an injection of 150 μL of 3mg/mL DiD-loaded nanoparticles through the tail vein. At each of the 24, 48, and 72 hour time points following the particle injection, 6 mice were randomly selected and euthanized. Their liver, kidney, spleen, brain, lung, heart and blood were collected. The collected organs were carefully weighed and then homogenized in 1 mL PBS. Total weight of blood was estimated as 6% of mouse body weight. The fluorescence intensity of each sample was determined by an Infinite M200 multiplate reader.

4.3 Results and Discussion

4.3.1 Preparation of RBC Membrane Coated NPs

The preparation process of the RBC membrane-coated nanoparticles is divided into two parts: membrane vesicle derivation from RBCs and vesicle-particle fusion (Fig. 4.2). The derivation of RBC membrane vesicles follows a previously reported method with slight modifications (139). Briefly, RBCs were first purified from the fresh blood of male ICR mice (6-8 wks) from Charles River Laboratories (Wilmington, MA) by centrifugation and PBS wash. The isolated RBCs then underwent membrane rupture in a hypotonic environment to remove its intracellular contents (Fig. 4.3). Next, the emptied RBCs were washed and extruded through 100 nm porous membranes to create RBC membrane-derived vesicles. To synthesize the

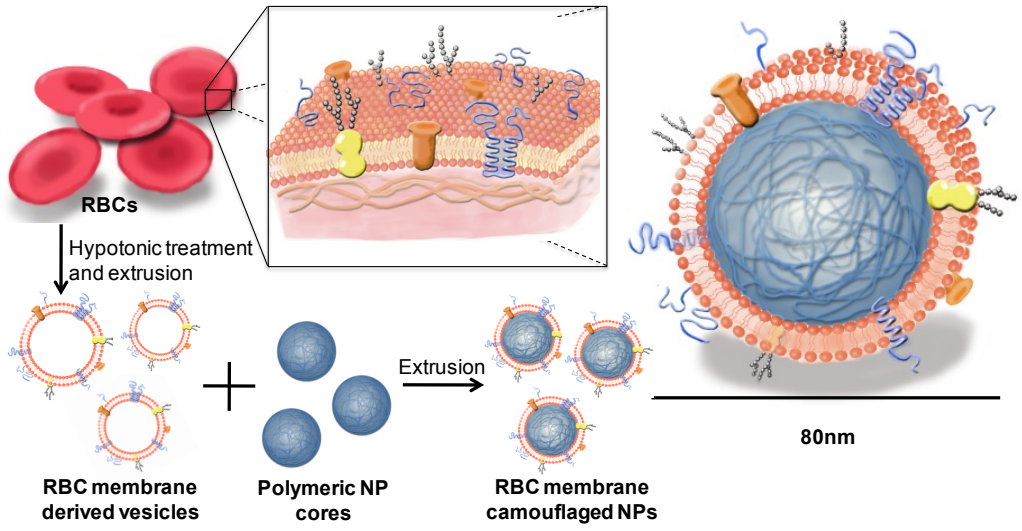


Fig. 4.2. Schematics of the preparation process of the RBC membrane-coated PLGA nanoparticles (NPs).

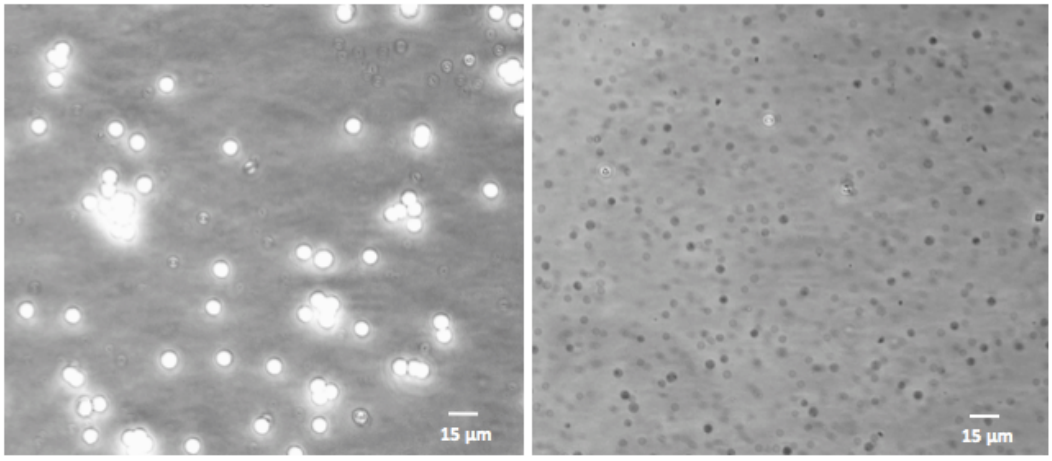


Fig. 4.3. Phase contrast microscopy images of mouse red blood cells (RBCs) before (left panel) and after (right panel) hemolytic treatment in hypotonic solution. Deprivation of RBC interior contents (hemoglobins) was verified by the change in phase contrast, which indicates an alteration of the medium inside the RBCs.

RBC membrane-camouflaged polymeric nanoparticles, PLGA particles of approximately 70 nm in diameter were first prepared from 0.67dL/g carboxyl-terminated PLGA polymer using a solvent displacement method (140). The resulting PLGA nanoparticles were subsequently fused with the RBC membrane-derived vesicles through mechanical extrusion. Based on calculations from PLGA polymer density, nanoparticle size, the erythrocyte lipid contents, and the estimated project area of a lipid molecule, each milligram of PLGA nanoparticles was mixed with vesicles derived from 1mL of blood for complete particle coating. The mixture was physically extruded through an apparatus with 100 nm pores. The mechanical force facilitated the sub-100 nm PLGA nanoparticles to cross the lipid bilayers, resulting in vesicle-particle fusion. Repeated passing through the extruder overcomes previously reported issues with liposome-particle fusion, such as broad particle size distribution, incomplete particle coating, and inconsistent lipid shells (141). It should also be noted that the bilayer structure of the RBC membranes is retained throughout the entire preparation process to minimize the loss of and damages to the membrane proteins. The size of the resulting products after each preparation step was followed using dynamic light scattering (DLS) (Fig. 4.4).

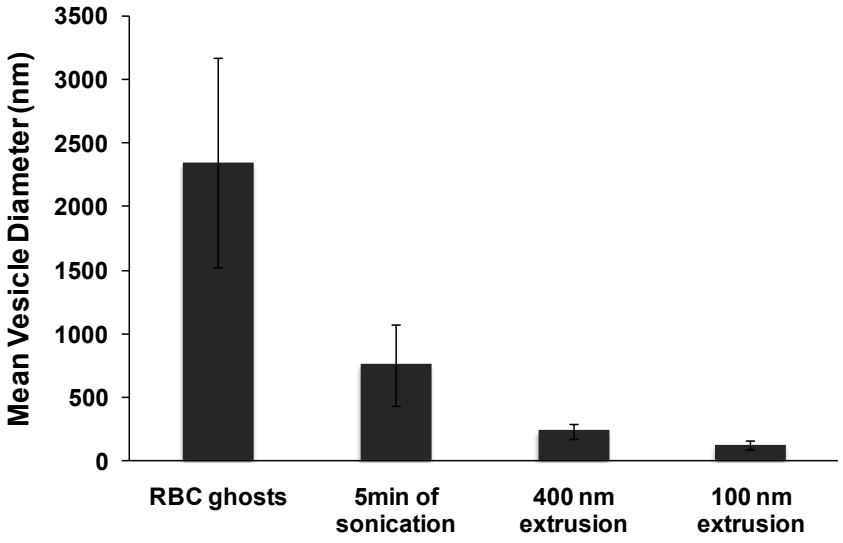


Fig. 4.4. The average diameter of the RBC membrane-derived vesicles following RBC ghosts derivation, 5 min of sonication, 400 nm extrusion, and 100 nm extrusion as measured by DLS.

4.3.2 Characterizations of RBC Membrane coated NPs

To characterize the RBC membrane-coated PLGA nanoparticles, the particles were first negatively stained with uranyl acetate and then visualized using transmission electron microscopy (TEM) (Fig. 4.5A). The resulting image reveals a core-shell structure as expected in a lipid bilayer-coated polymeric particle. The particle size is ~80 nm and matches the hydrodynamic diameter measured by dynamic light scattering (DLS). Closer examination reveals a polymeric core approximately 70 nm in diameter and an outer lipid shell 7~8 nm in thickness. The thickness of the lipid layer is in agreement with the reported membrane width of

RBCs (142), suggesting a successful membrane translocation to the polymeric particle surface.

To examine the long-term stability of the resulting RBC-mimicking nanoparticles, they were suspended in 1X PBS at a concentration of 1mg/mL and then monitored by DLS for the particle size, the polydispersity index (PDI), and the zeta potential (Fig. 4.5B). Over a span of two weeks the particle size increased from 85 to 130 nm, the zeta potential decreased from -10.2 to -12.7 mV, and the PDI remained relatively the same at 0.26. The changes in size and zeta potential are likely caused by the fusion of small amount of excess vesicles in the particle solution. To verify the integrity of the core-shell particle structure, hydrophobic DiD fluorophore (excitation/emission = 644 nm/655 nm) and the lipophilic rhodamine-DMPE dye (excitation/emission = 557 nm/571 nm) were loaded into the polymeric core and the RBC membrane-derived vesicles, respectively, prior to the vesicle-particle fusion. The resulting dual-fluorophore labeled nanoparticles were incubated with HeLa cells for 6 hours and visualized using fluorescence microscopy. In Fig. 4.5C, DiD (red) and rhodamine-DMPE (green), each of which corresponds to a different particle compartment, overlap in the same locations. This fluorescence co-localization indicates an intact core-shell structure of the nanoparticles after they are internalized by the cells.

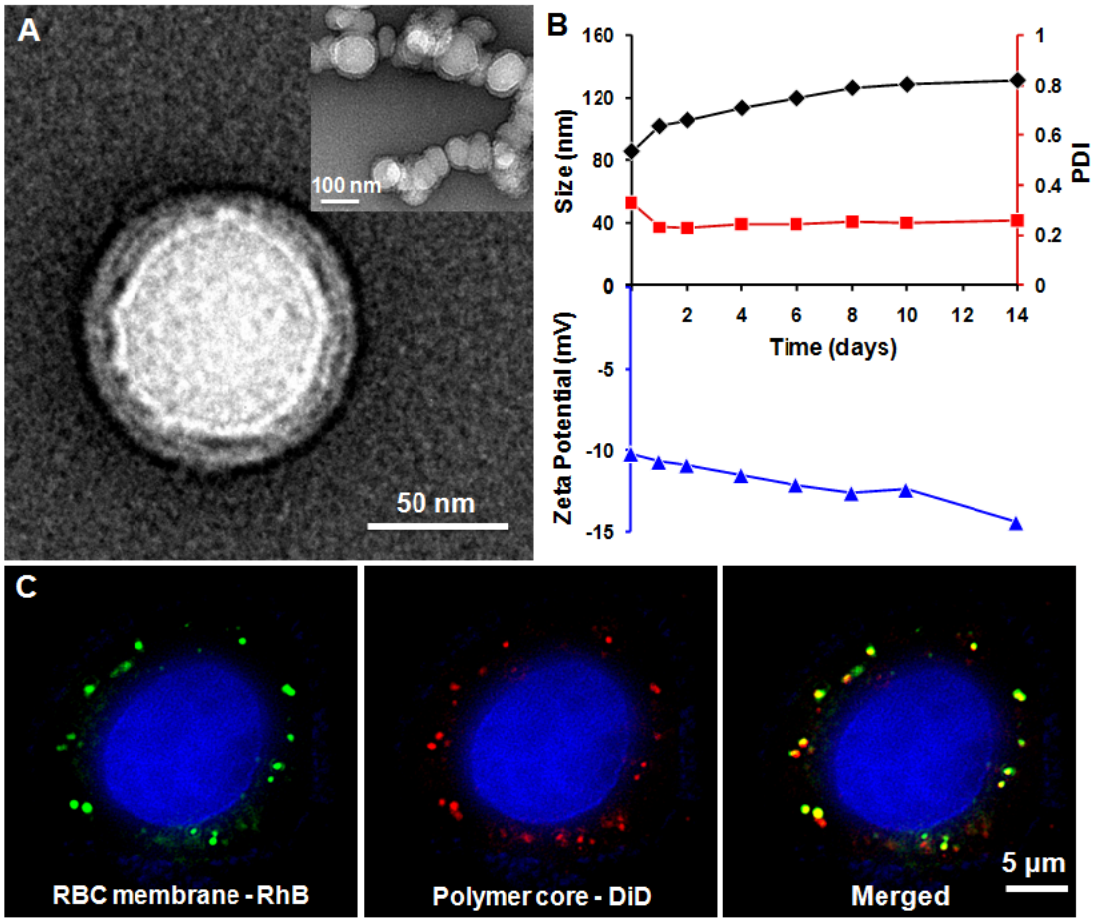


Fig. 4.5. Structural characterization of the RBC membrane-coated PLGA nanoparticles. (A) The nanoparticles were negatively stained with uranyl acetate and subsequently visualized with TEM. (B) DLS measurements of the size, polydispersity index (PDI), and surface zeta potential of the nanoparticles over 14 days. (C) Scanning fluorescence microscopy images demonstrated the co-localization of the RBC membranes (visualized with green rhodamine-DMPE dyes) and polymeric cores (visualized with red DiD dyes) after being internalized by HeLa cells. The RBC membrane-coated nanoparticles were incubated with HeLa cells for 6 hours. The excess nanoparticles were washed out and the cells were subsequently fixed for imaging.

Following the structural studies, the particles were examined for their protein contents. The RBC membrane-coated nanoparticles were dialyzed with 30 nm porous membranes for 24 hours to remove unbound proteins and subsequently treated with sodium dodecyl sulfate (SDS) to solubilize the membrane proteins. Samples of emptied RBCs and RBC membrane-derived vesicles were prepared in parallel as a comparison. Protein separation by polyacrylamide gel electrophoresis (PAGE) indicates that the composition of membrane proteins were mostly retained throughout the particle synthesis and can be identified on the RBC membrane-coated PLGA nanoparticles (Fig. 4.6A). This finding suggests that the translocation of the bilayered cellular membranes also transfers the associated membrane proteins to the nanoparticle surface. Since the solid PLGA core precludes protein entries and unbound proteins are filtered out by dialysis, the detected membrane proteins are most likely anchored in the bilayered lipid membranes that surround the nanoparticles. The resulting protein-containing lipid membrane-coated particles can be likened to a well-studied polymer-supported planer lipid bilayer model, which has been shown to retain the functionalities of membrane-associated proteins (141). Minor alteration in the protein makeup, however, was observed as a band near 51kDa is noticeably fainter. The faint band likely corresponds to peripheral membrane proteins associated with spectrin cytoskeletal proteins, which are lost during the mechanical extrusion for the vesicle-particle fusion as can be observed by the missing band at ~200kDa.

4.3.3 Stability and Circulation Half-life of RBC Membrane Coated NPs

We then investigated the serum stability and the *in vivo* circulation half-life of the RBC membrane-coated nanoparticles. To put the results into perspective, similarly sized bare PLGA nanoparticles (~75 nm) and structurally analogous PEG (Mw 2000)-functionalized lipid-polymer hybrid nanoparticles (~80 nm) were used as negative and positive controls respectively. For the serum stability test, a previously cited absorbance method was used to monitor the particle size change in the presence of fetal bovine serum (FBS) (143, 144). Since larger particles induce higher light scattering, aggregation of unstable particles can be observed by monitoring the increase in the absorbance value. Each type of the nanoparticles were suspended in 100% FBS with a final nanoparticle concentration of 1 mg/mL. All samples were incubated at 37°C and shaked gently prior to each absorbance measurement. The absorbance values measured at 560 nm suggest that the RBC-membrane coated nanoparticles have equivalent serum stability as the PEG-functionalized lipid-polymer hybrid nanoparticles as neither sample showed any observable change in absorbance within 4 hours (Fig. 4.6B). In contrast, the bare PLGA nanoparticles showed little stability as they immediately aggregated upon mixture with the serum solution.

To study the systemic circulation time of the each type of nanoparticles, we loaded the hydrophobic DiD fluorescent dye to all three types of nanoparticles. The dye shows minimal release (<20% in 72hours) and has been widely cited as a marker for the circulation studies of nanoparticles (145, 146). For each particle type, 150 μL

of 3 mg/mL DiD-loaded nanoparticles were injected into a group of 6 mice through tail-vein injection. To avoid the immune responses associated with different blood types, the mice subject to the circulation studies are of the same strain from which the RBCs are collected to prepare the nanoparticles. At various time points following the injection, 20 μL blood were collected from the eye socket of the mice for fluorescence measurements. Fig. 4.6C shows that the RBC membrane-coated nanoparticles had superior blood retention to the PEG-functionalized nanoparticles. At 24 and 48 hour marks, the RBC membrane-coated nanoparticles exhibited 29% and 16% overall retention respectively as compared to the 11% and 2% exhibited by the PEG-coated nanoparticles. The bare PLGA nanoparticles, on the other hand, showed negligible signal in the first blood withdrawal at the 2 minute mark, which was expected based on their rapid aggregations in serum. The semi-log plot in the inset of Fig. 4.6C better illustrates the difference in the pharmacokinetic profiles as circulation half-life can be derived from the slope of the semi-log signals. Based on a two-compartment model that has been applied in previous studies to fit the circulation results of nanoparticles (147, 148), the elimination half-life was calculated as 39.6 hours for the RBC membrane-coated nanoparticles and 15.8 hours for the PEG-coated nanoparticles. Alternatively, the circulation data in Fig. 4.6C can be interpreted through a one-way non-linear clearance model, where the causes of nanoparticle clearance (i.e. availability of clearing sites and opsonin proteins) are continuously depleted to give rise to a slowing particle uptake. Simberg *et al.* have reported that by injecting “decoy” particles prior to the injection of primary particles, the circulation

half-life of the primary particles can be prolonged by nearly 5-fold (149). It is reasonable to expect that the saturation of the RES system can retard additional particle uptake and account for a non-linear particle elimination rate. Based on this non-linear elimination model, the first apparent half-life (i.e., 50% of the particles are cleared) is 9.6 hours for the RBC membrane-coated nanoparticles and 6.5 hours for the PEG-coated nanoparticles. Regardless of the pharmacokinetic models, the RBC membrane-coated nanoparticles have longer elimination half-life, which suggests that the RBC membrane coating is superior in retarding *in vivo* clearance compared to the conventional PEG stealth coating. This finding further confirms that the nanoparticles were modified with the functional components on the RBC membranes, which contain immunosuppressive proteins that inhibit macrophage uptake (150). Since these membrane proteins are from the natural RBCs collected from the host blood, they are expected to stimulate negligible immune response after they are translocated to the surface of polymeric nanoparticles. With the TEM visualization, the SDS-PAGE results, and the circulation half-life study, we demonstrate the transfer of cell membranes and the corresponding functional surface proteins for nanoparticle functionalization using the reported technique.

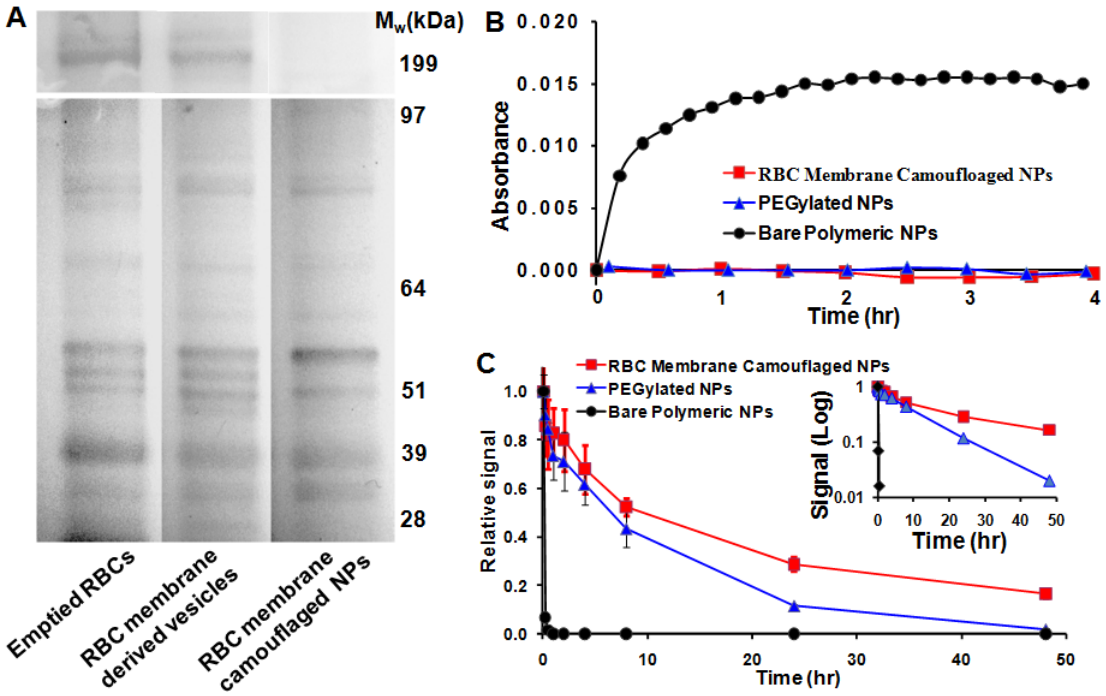


Fig. 4.6. Membrane protein retention, particle stability in serum, and the *in vivo* circulation time of the RBC membrane-coated nanoparticles (NPs). (A) Proteins in emptied RBCs, RBC membrane-derived vesicles, and purified RBC membrane-coated PLGA nanoparticles were solubilized and resolved on a polyacrylamide gel. (B) RBC membrane-coated PLGA nanoparticles, PEG-coated lipid-PLGA hybrid nanoparticles, and bare PLGA nanoparticles were incubated in 100% fetal bovine serum and monitored for absorbance at 560 nm for 4hours. (C) DiD-loaded nanoparticles were injected intravenously through the tail vein of mice. At various time points blood was withdrawn intraorbitally and measured for fluorescence at 670 nm to evaluate the systemic circulation lifetime of the nanoparticles (n=6 per group).

4.3.4 Biodistributions of RBC Membrane Coated NPs

Finally we investigated the *in vivo* tissue distribution of the RBC membrane-coated nanoparticles to further evaluate their potential as a delivery vehicle. For the biodistribution study, 18 mice received an injection of 150 μL of 3mg/mL DiD-loaded nanoparticles through the tail vein. At each of the 24, 48, and 72 hour time points following the particle injection, 6 mice were euthanized and their liver, kidney, spleen, brain, lung, heart and blood were collected. For fluorescence quantification, the organs collected at different time points were washed, weighed, homogenized in 1 mL PBS, and then measured by a fluorospectrometer. Fig. 4.7A shows the nanoparticle content per gram of tissue. The two primary organs of the RES system, liver and spleen, contained the highest amount of nanoparticles. However, significant fluorescent level was also observed in the blood at the 3 time points. To better understand the overall particle distribution, the fluorescence signals were multiplied by the measured weight of the corresponding organs, with the weight of the blood being estimated as 6% of the total body weight. Fig. 4.7B shows relative signal in each organ normalized to the total fluorescence. After accounting for the tissue mass, it can be observed that the nanoparticles are distributed mainly in the blood and the liver. The fluorescence signals from the blood correlate well with the data from the circulation half-life study, with 21%, 15%, and 11% of nanoparticle retention at 24, 48, and 72 hour marks respectively. Also, as the blood fluorescence decreased, a corresponding increase in signal was observed in the liver, which indicates that the source of the fluorescence in the blood was eventually taken up by the RES system.

This result validates that the observed blood fluorescence came from the long-circulating nanoparticles rather than leakage of the dye, which would be secreted by the kidneys and result in a reduction in the signal intensity from the liver. It is worth noting that the RBC membrane-coated polymeric nanoparticles have a significantly longer circulation time compared to previously reported RBC-derived liposomes, which are cleared from the blood circulation in less than 30 minutes (139). This prolonged circulation time by the RBC membrane-coated nanoparticles can be attributed to the higher structural rigidity, better particle stability, and the more reliable cargo/dye encapsulation. As compared to other published data on nanoparticle circulations in mice models (140, 151, 152), most of which show negligible blood retention after 24 hours, the RBC membrane-coated nanoparticles exhibit superior *in vivo* residence time and hold tremendous potentials for biomedical applications as a robust delivery platform.

The erythrocyte membrane-coated nanoparticles reported herein are structurally analogous to the commonly cited lipid-polymer hybrid nanoparticles, which are quickly emerging as a promising multi-functional drug delivery platform that contains the desirable characteristics of both liposomes and polymeric nanoparticles (153, 154). Lipid-polymer hybrid nanoparticles have shown a more sustained drug release profile compared to polymeric nanoparticles with similar size owing to the diffusional barrier provided by the lipid monolayer coating. The drug release kinetics from the RBC membrane-coated nanoparticles is expected to be even more gradual because the RBC membrane provides a more dense and bilayered lipid

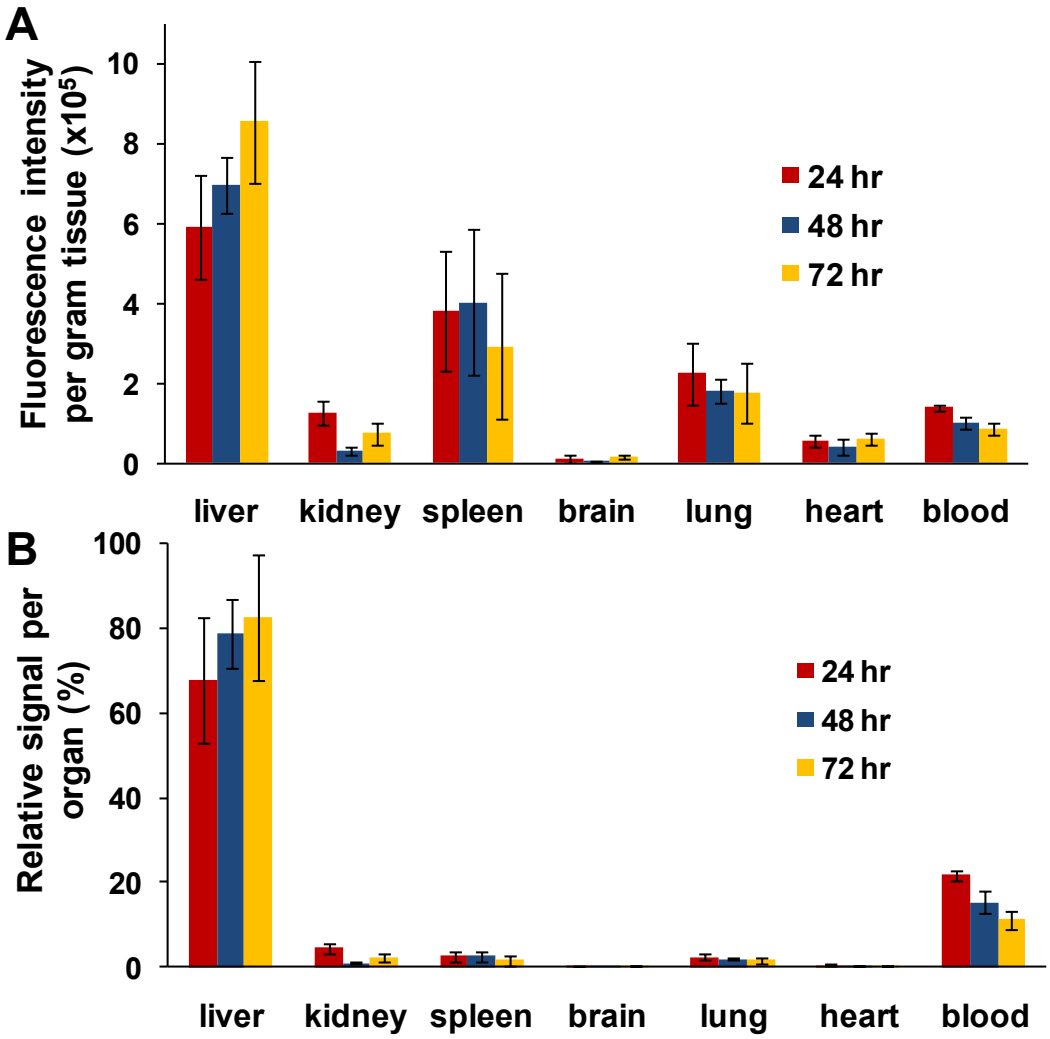


Fig. 4.7. Biodistributions of the RBC membrane-coated polymeric nanoparticles. Fluorescently labeled nanoparticles were injected intravenously into the mice. At each time points (24, 48, and 72 hour respectively), the organs from a randomly grouped subset of mice were collected, homogenized and quantified for fluorescence. (A) Fluorescence intensity per gram of tissue (n=6 per group). (B) Relative signal per organ.

barrier against drug diffusion. The membrane coating approach in this study can also be extended to other nanostructures as the versatility of lipid coating has made its way to silica nanoparticles and quantum dots (155-157). Further particle functionalization can be achieved by inserting modified lipids, lipid derivatives, or transmembrane proteins to the lipid membranes prior to the preparation of the RBC membrane-coated nanostructures.

Regarding the translation of these RBC membrane-coated nanoparticles as a clinical drug delivery vehicle, many challenges and opportunities lie ahead. Unlike in animal studies human erythrocytes contain numerous surface antigens that can be classified to many different blood groups. To optimize the particles for long-circulating drug delivery, the particles need to be cross-matched to patients' blood as in the case of blood transfusion. For more versatile applications to broad populations of patients, the particles can be selectively depleted of those immunogenic proteins during the synthesis steps. Alternatively, this biomimetic delivery platform could be an elegant method for personalized medicine whereby the drug delivery nanocarrier is tailored to individual patients with little risk of immunogenicity by using their own RBC membranes as the particle coatings.

4.4 Conclusions

In conclusions, we demonstrate the synthesis of an erythrocyte membrane-camouflaged polymeric nanoparticle for long-circulating cargo delivery. The adopted technique aims to fabricate cell-mimicking nanoparticles through a top-down approach which bypasses the labor-intensive processes of protein identifications, purifications, and conjugations. The proposed method also provides a bilayered medium for transmembrane protein anchorage and avoids chemical modifications which could compromise the integrity and functionalities of target proteins. We demonstrate that the lipid layer can be derived directly from live cells. The translocation of natural cellular membranes and their associated functionalities to the particle surface represents a unique and robust top-down approach in nanoparticle functionalization.

Chapter 4, in full, is a reprint of the material as it appears in Proceedings of the National Academy of Sciences, 2011, Che-Ming Hu, Li Zhang, Santosh Aryal, Connie Cheung, Ronnie H. Fang, and Liangfang Zhang. The dissertation author was the primary investigator and author of this paper.

Chapter 5 Conclusions and Future Directions

NPs have shown great promises in breaking down the various barriers in cancer drug delivery. On the physiological level, long-circulating NPs can take advantage of the EPR effects in solid tumors and enhance tumoral accumulation through passive targeting. NPs functionalized with tumor-targeted ligands have demonstrated increased target selectivity and are able to facilitate the breaching of cellular membrane barriers through receptor-mediated endocytosis. On the molecular level, multi-drug loaded NPs can further improve treatment efficacy by targeting multiple molecular pathways and retard the development of cancer drug resistance. The promises of anticancer therapeutic NPs have drawn significant attention from clinicians, scientists, and engineers. The work of this dissertation aims to present important improvements in three specific areas of therapeutic NPs:

1. Enabling facile assembly of multi-drug NPs with ratiometrically controllable drug loading through drug-polymer conjugates.

2. Enabling robust, site-specific NP functionalization for targeted drug delivery through the use of reduced half-antibodies.

3. Enabling long-circulating delivery with little risk of immunogenic response through red blood cell membrane coating to camouflage NPs.

The results presented here add significant contributions to the continuing development of therapeutic NPs. While functionally distinct, each of the aforementioned developments is structurally compatible with one another. The half-antibodies and the RBC membrane coating techniques are also compatible with other nanostructures, providing additional toolkit to the fledging field of nanotechnology and nanomedicine. The following sections will reiterate the important conclusions from this dissertation.

5.1 Drug-polymer Conjugates for Facile Assembly of Ratiometrically Controlled Multidrug NPs

To address the batch-to-batch variability in non-covalent multi-drug encapsulation in polymeric NPs, different drug molecules were conjugated to a long biodegradable PLA chain prior to NP preparation. Using ring opening polymerization, two anticancer drugs, DOX and CPT with different physicochemical properties, were attached a hydrophobic polymer chain with uniform length and property. The

resulting drug-polymer conjugates were used to prepare NPs and formulations with various DOX-PLA and CPT-PLA ratios, yielding NPs with consistent size at approximately 100 nm. Drug quantification study showed that the final NP formulations contained the same drug-to-drug ratio as the polymer mixture used during the NP preparation. Owing to the distinct spectral properties of DOX and CPT, fluorescence microscopy was used to confirm the colocalization of the two drugs upon cellular engulfment of the NPs, verifying the presence of both drugs within each single NP.

In vitro Cytotoxicity study revealed that the potency of the NP formulation is highly dependent on the drug-to-drug ratio between the two drug types. In addition, it was found that the NP-based combination therapy consistently outperformed the cocktail mixture of single-drug NPs in therapeutic efficacy. The findings showed the advantage of multi-drug NPs, which would benefit from robust drug-polymer conjugate platform.

5.2 Half-antibody for Regioselective Nanoparticle Functionalization and Tumor Targeting

To improved drug delivery to pancreatic cancer, which is poorly vascularized, NPs were functionalized with anti-CEA half-antibodies to target the tumor-associated CEA antigens. A low molar excess of TCEP was used to selectively reduce the interchain disulfide bonds located at the hinge region of

IgG antibodies for the creation of hAb fragments for regioselective conjugation. The disulfide bond reduction generated sulfhydryl groups at the non-active region of the half antibodies. Maleimide-functionalized NPs were incubated with the hAb fragment and site-specific conjugation was achieved through thiol-maleimide bond formation without interfering with the active regions at the binding sites of the antibodies.

Production of the hAb fragments with antigen-binding ability was verified using SDS-PAGE and fluorescence microscopy. Through fluorescence colocaliztion we showed that the hAb and NPs were attached. Fluorescent quantification showed that on each 85-nm particle there were approximately 25 hAb fragments. The targeted NPs were highly stable as the hAb-NPs attachment was intact upon cellular internalization. The resulting anti-CEA NPs showed selective cellular uptake by the CEA-presenting pancreatic cancer cells. In the cytotoxicity study where NPs were loaded with paclitaxel, the targeted NPs showed superior toxicity as opposed to the non-targeted NPs. The study demonstrated the benefit of active targeting in cancer drug delivery. It also presented the hAb as a highly applicable approach for antibody functionalization, which could be applied to a variety of biomedical applications.

5.3 Red blood cell Membrane Coating to Extend Nanoparticle Circulation in vivo

The RBC membrane coating on NPs presents a revolutionary approach in long-circulating NPs. Traditional stealth strategies surround nanoparticles with highly hydrophilic polymers to create a hydration shell in aim to render them invisible to the immune system. The RBC membrane coating on the other hand takes advantage of the membrane properties of the natural, endogenous red blood cells to camouflage the NPs as "self" entities. Translocations of RBC membranes, surface protein markers, and their functionalities on NPs were achieved using a non-disruptive mechanical extrusion method. The resulting NPs possessed the same exterior as that of RBCs.

The RBC NPs were shown to be highly stable both *in vitro* and *in vivo*. The particles remained in suspension in PBS for two weeks and had superior circulation half-life as compared to PEGylated NPs. Using a two-compartment pharmacokinetic model, the RBC NPs had a circulation half-life of approximately 40hr in mice as opposed to 16hr by the PEGylated NPs. Biodistributions studies showed that overtime the NPs were removed from the blood circulation by the liver. As opposed to the stealth moieties based on hydrophilic polymers, the RBC coating approach offers the opportunity for personalized NP camouflage and poses minimal risk of immunogenicity. The PLGA polymeric core used as the colloidal support for the RBC membrane can encapsulate a variety of theranostic agents for clinical applications. In addition, the membrane coating technique could be translated to other nanoscale platforms.

REFERENCES

1. Jain RK. Barriers to drug delivery in solid tumors. Sci Am. 1994;271(1):58-65.

2. Bugnon D, Giannoni E, Majcherczyk P, Glauser MP, Moreillon P. Pitfalls in cefepime titration from human plasma: plasma- and temperature-related drug degradation in vitro. Antimicrob Agents Chemother. 2002;46(11):3654-6.

3. Mosnaim AD, Wolf ME, Nguyen TD, Puente J, Freitag F, Diamond S. Degradation kinetics of leucine5-enkephalin by plasma samples from healthy controls and various patient populations: in vitro drug effects. Am J Ther. 2000;7(3):185-94.

4. Geisslinger G, Menzel S, Brune K. Stereospecific determination of tiaprofenic acid in plasma: problems with drug degradation. J Chromatogr B Biomed Appl. 1996;675(1):77-81.

5. Carrstensen H, Muller RH, Muller BW. Particle size, surface hydrophobicity and interaction with serum of parenteral fat emulsions and model drug carriers as parameters related to RES uptake. Clin Nutr. 1992;11(5):289-97.

6. Nagai K, Ito Y, Otsuka N, Muranaka A, Kaji T, Kajihara Y. Experimental studies on uptake of 99mTc-antimony sulfide colloid in RES--a comparison with various 99mTc-colloids. Int J Nucl Med Biol. 1981;8(1):85-9.

7. Janku I, Zvara K. Quantitative analysis of drug handling by the kidney using a physiological model of renal drug clearance. Eur J Clin Pharmacol. 1993;44(6):521-4.

8. Janku I. Physiological modelling of renal drug clearance. Eur J Clin Pharmacol. 1993;44(6):513-9.

9. Lalka D, du Souich P, McLean AJ, Gibaldi M. Absolute drug bioavailability II: Evaluation of renal clearance perturbation method using literature data assuring a fraction absorbed of unity. J Pharm Sci. 1978;67(4):591-2.

10. Lelievre L, Paraf A, Charlemagne D, Sheppard JR. Plasma membrane studies on drug sensitive and resistant cell lines. I. Cross resistance and membrane enzyme coordination (ouabain/cAMP/Na+/K+ ATPase/adenylate cyclase). Exp Cell Res. 1977;104(1):191-7.

11. Bassolino D, Alper H, Stouch TR. Drug-membrane interactions studied by molecular dynamics simulation: size dependence of diffusion. Drug Des Discov. 1996;13(3-4):135-41.

12. Nagengast WB, Oude Munnink TH, Dijkers EC, Hospers GA, Brouwers AH, Schroder CP, et al. Multidrug resistance in oncology and beyond: from imaging of drug efflux pumps to cellular drug targets. Methods Mol Biol. 2010;596:15-31.

13. Lomovskaya O, Watkins W. Inhibition of efflux pumps as a novel approach to combat drug resistance in bacteria. J Mol Microbiol Biotechnol. 2001;3(2):225-36.

14. Woodcock J, Griffin JP, Behrman RE. Development of novel combination therapies. N Engl J Med. 2011;364(11):985-7.

15. Gottesman MM. Mechanisms of cancer drug resistance. Annu Rev Med. 2002;53:615-27.

16. Couvreur P, Vauthier C. Nanotechnology: intelligent design to treat complex disease. Pharmacol Res. 2006;23(7):1417-50.

17. Davis ME, Chen ZG, Shin DM. Nanoparticle therapeutics: an emerging treatment modality for cancer. Nat Rev Drug Discov. 2008;7(9):771-82.

18. Zhang L, Gu FX, Chan JM, Wang AZ, Langer RS, Farokhzad OC. Nanoparticles in medicine: therapeutic applications and developments. Clin Pharmacol Ther. 2008;83(5):761-9.

19. Peer D, Karp JM, Hong S, Farokhzad OC, Margalit R, Langer R. Nanocarriers as an emerging platform for cancer therapy. Nat Nanotechnol. 2007;2(12):751-60.

20. Maeda H. The enhanced permeability and retention (EPR) effect in tumor vasculature: the key role of tumor-selective macromolecular drug targeting. Adv Enzyme Regul. 2001;41:189-207.

21. Matsumura Y, Maeda H. A new concept for macromolecular therapeutics in cancer chemotherapy: mechanism of tumoritropic accumulation of proteins and the antitumor agent smancs. Cancer Res. 1986;46(12 Pt 1):6387-92.

22. Tanaka T, Shiramoto S, Miyashita M, Fujishima Y, Kaneo Y. Tumor targeting based on the effect of enhanced permeability and retention (EPR) and the

mechanism of receptor-mediated endocytosis (RME). Int J Pharm. 2004;277(1-2):39-61.

23. Torchilin VP. Recent advances with liposomes as pharmaceutical carriers. Nat Rev Drug Discov. 2005;4(2):145-60.

24. Ballou B, Lagerholm BC, Ernst LA, Bruchez MP, Waggoner AS. Noninvasive imaging of quantum dots in mice. Bioconjug Chem. 2004;15(1):79-86.

25. Carpenter CP, Woodside MD, Kinkead ER, King JM, Sullivan LJ. Response of dogs to repeated intravenous injection of polyethylene glycol 4000 with notes on excretion and sensitization. Toxicol Appl Pharmacol. 1971;18(1):35-40.

26. Uchida K, Otsuka H, Kaneko M, Kataoka K, Nagasaki Y. A reactive poly(ethylene glycol) layer to achieve specific surface plasmon resonance sensing with a high S/N ratio: the substantial role of a short underbrushed PEG layer in minimizing nonspecific adsorption. Anal Chem. 2005;77(4):1075-80.

27. Jiang W, Kim BYS, Rutka JT, Chan WCW. Nanoparticle-mediated cellular response is size-dependent. Nat Nanotechnol. 2008;3(3):145-50.

28. Perrault SD, Walkey C, Jennings T, Fischer HC, Chan WC. Mediating tumor targeting efficiency of nanoparticles through design. Nano Lett. 2009;9(5):1909-15.

29. Gabizon A, Shmeeda H, Barenholz Y. Pharmacokinetics of pegylated liposomal Doxorubicin: review of animal and human studies. Clin Pharmacokinet. 2003;42(5):419-36.

30. Li Y, Pei Y, Zhang X, Gu Z, Zhou Z, Yuan W, et al. PEGylated PLGA nanoparticles as protein carriers: synthesis, preparation and biodistribution in rats. J Control Release. 2001;71(2):203-11.

31. Peracchia MT, Fattal E, Desmaele D, Besnard M, Noel JP, Gomis JM, et al. Stealth PEGylated polycyanoacrylate nanoparticles for intravenous administration and splenic targeting. J Control Release. 1999;60(1):121-8.

32. Park JW, Kirpotin DB, Hong K, Shalaby R, Shao Y, Nielsen UB, et al. Tumor targeting using anti-her2 immunoliposomes. J Control Release. 2001;74(1-3):95-113.

33. Kamps JA, Koning GA, Velinova MJ, Morselt HW, Wilkens M, Gorter A, et al. Uptake of long-circulating immunoliposomes, directed against colon

adenocarcinoma cells, by liver metastases of colon cancer. J Drug Target. 2000;8(4):235-45.

34. Sapra P, Allen TM. Internalizing antibodies are necessary for improved therapeutic efficacy of antibody-targeted liposomal drugs. Cancer Res. 2002;62(24):7190-4.

35. Maruyama K, Ishida O, Takizawa T, Moribe K. Possibility of active targeting to tumor tissues with liposomes. Adv Drug Deliv Rev. 1999;40(1-2):89-102.

36. Zhou Y, Drummond DC, Zou H, Hayes ME, Adams GP, Kirpotin DB, et al. Impact of single-chain Fv antibody fragment affinity on nanoparticle targeting of epidermal growth factor receptor-expressing tumor cells. J Mol Biol. 2007;371(4):934-47.

37. Drummond DC, Hong K, Park JW, Benz CC, Kirpotin DB. Liposome targeting to tumors using vitamin and growth factor receptors. Vitam Horm. 2000;60:285-332.

38. Stella B, Arpicco S, Peracchia MT, Desmaele D, Hoebeke J, Renoir M, et al. Design of folic acid-conjugated nanoparticles for drug targeting. J Pharm Sci. 2000;89(11):1452-64.

39. Farokhzad OC, Cheng J, Teply BA, Sherifi I, Jon S, Kantoff PW, et al. Targeted nanoparticle-aptamer bioconjugates for cancer chemotherapy in vivo. Proc Natl Acad Sci USA. 2006;103(16):6315-20. PMCID: 1458875.

40. Karmali PP, Kotamraju VR, Kastantin M, Black M, Missirlis D, Tirrell M, et al. Targeting of albumin-embedded paclitaxel nanoparticles to tumors. Nanomedicine. 2009;5(1):73-82.

41. Laakkonen P, Porkka K, Hoffman JA, Ruoslahti E. A tumor-homing peptide with a targeting specificity related to lymphatic vessels. Nat Med. 2002;8(7):751-5.

42. Montet X, Funovics M, Montet-Abou K, Weissleder R, Josephson L. Multivalent effects of RGD peptides obtained by nanoparticle display. J Med Chem. 2006;49(20):6087-93.

43. Koval M, Preiter K, Adles C, Stahl PD, Steinberg TH. Size of IgG-opsonized particles determines macrophage response during internalization. Exp Cell Res. 1998;242(1):265-73.

44. Rejman J, Oberle V, Zuhorn IS, Hoekstra D. Size-dependent internalization of particles via the pathways of clathrin- and caveolae-mediated endocytosis. Biochem J. 2004;377(Pt 1):159-69. PMCID: 1223843.

45. Huwyler J, Cerletti A, Fricker G, Eberle AN, Drewe J. By-passing of P-glycoprotein using immunoliposomes. J Drug Target. 2002;10(1):73-9.

46. Rapoport N, Marin A, Luo Y, Prestwich GD, Muniruzzaman MD. Intracellular uptake and trafficking of Pluronic micelles in drug-sensitive and MDR cells: effect on the intracellular drug localization. J Pharm Sci. 2002;91(1):157-70.

47. Sahoo SK, Labhasetwar V. Enhanced antiproliferative activity of transferrin-conjugated paclitaxel-loaded nanoparticles is mediated via sustained intracellular drug retention. Mol Pharm. 2005;2(5):373-83.

48. Thierry AR, Vige D, Coughlin SS, Belli JA, Dritschilo A, Rahman A. Modulation of doxorubicin resistance in multidrug-resistant cells by liposomes. FASEB J. 1993;7(6):572-9.

49. DeVita VT, Jr., Young RC, Canellos GP. Combination versus single agent chemotherapy: a review of the basis for selection of drug treatment of cancer. Cancer. 1975;35(1):98-110.

50. Pavillard V, Kherfellah D, Richard S, Robert J, Montaudon D. Effects of the combination of camptothecin and doxorubicin or etoposide on rat glioma cells and camptothecin-resistant variants. Br J Cancer. 2001;85(7):1077-83.

51. Raitanen M, Rantanen V, Kulmala J, Helenius H, Grenman R, Grenman S. Supra-additive effect with concurrent paclitaxel and cisplatin in vulvar squamous cell carcinoma in vitro. Int J Cancer. 2002;100(2):238-43.

52. Bayne WF, Mayer LD, Swenson CE. Pharmacokinetics of CPX-351 (cytarabine/daunorubicin HCl) liposome injection in the mouse. J Pharm Sci. 2009;98(7):2540-8.

53. Lim WS, Tardi PG, Dos Santos N, Xie X, Fan M, Liboiron BD, et al. Leukemia-selective uptake and cytotoxicity of CPX-351, a synergistic fixed-ratio cytarabine:daunorubicin formulation, in bone marrow xenografts. Leuk Res. 2010;34(9):1214-23.

54. Feldman EJ, Lancet JE, Kolitz JE, Ritchie EK, Roboz GJ, List AF, et al. First-in-man study of CPX-351: a liposomal carrier containing cytarabine and daunorubicin in a fixed 5:1 molar ratio for the treatment of relapsed and refractory acute myeloid leukemia. J Clin Oncol. 2011;29(8):979-85.

55. Batist G, Gelmon KA, Chi KN, Miller WH, Jr., Chia SK, Mayer LD, et al. Safety, pharmacokinetics, and efficacy of CPX-1 liposome injection in patients with advanced solid tumors. Clin Cancer Res. 2009;15(2):692-700.

56. Soma CE, Dubernet C, Bentolila D, Benita S, Couvreur P. Reversion of multidrug resistance by co-encapsulation of doxorubicin and cyclosporin A in polyalkylcyanoacrylate nanoparticles. Biomaterials. 2000;21(1):1-7.

57. Ganta S, Amiji M. Coadministration of Paclitaxel and curcumin in nanoemulsion formulations to overcome multidrug resistance in tumor cells. Mol Pharm. 2009;6(3):928-39.

58. Patel NM, Nozaki S, Shortle NH, Bhat-Nakshatri P, Newton TR, Rice S, et al. Paclitaxel sensitivity of breast cancer cells with constitutively active NF-kappaB is enhanced by IkappaBalpha super-repressor and parthenolide. Oncogene. 2000;19(36):4159-69.

59. van Vlerken LE, Duan Z, Seiden MV, Amiji MM. Modulation of intracellular ceramide using polymeric nanoparticles to overcome multidrug resistance in cancer. Cancer Res. 2007;67(10):4843-50.

60. Li X, Lu WL, Liang GW, Ruan GR, Hong HY, Long C, et al. Effect of stealthy liposomal topotecan plus amlodipine on the multidrug-resistant leukaemia cells in vitro and xenograft in mice. Eur J Clin Invest. 2006;36(6):409-18.

61. Liang GW, Lu WL, Wu JW, Zhao JH, Hong HY, Long C, et al. Enhanced therapeutic effects on the multi-drug resistant human leukemia cells in vitro and xenograft in mice using the stealthy liposomal vincristine plus quinacrine. Fundam Clin Pharmacol. 2008;22(4):429-37.

62. Patel NR, Rathi A, Mongayt D, Torchilin VP. Reversal of multidrug resistance by co-delivery of tariquidar (XR9576) and paclitaxel using long-circulating liposomes. Int J Pharm. 2011;416(1):296-9.

63. Wu J, Lu Y, Lee A, Pan X, Yang X, Zhao X, et al. Reversal of multidrug resistance by transferrin-conjugated liposomes co-encapsulating doxorubicin and verapamil. J Pharm Pharm Sci. 2007;10(3):350-7.

64. Saad M, Garbuzenko OB, Minko T. Co-delivery of siRNA and an anticancer drug for treatment of multidrug-resistant cancer. Nanomedicine (Lond). 2008;3(6):761-76.

65. Wang Y, Gao S, Ye WH, Yoon HS, Yang YY. Co-delivery of drugs and DNA from cationic core-shell nanoparticles self-assembled from a biodegradable copolymer. Nat Mater. 2006;5(10):791-6.

66. Song XR, Cai Z, Zheng Y, He G, Cui FY, Gong DQ, et al. Reversion of multidrug resistance by co-encapsulation of vincristine and verapamil in PLGA nanoparticles. Eur J Pharm Sci. 2009;37(3-4):300-5.

67. Patil Y, Sadhukha T, Ma L, Panyam J. Nanoparticle-mediated simultaneous and targeted delivery of paclitaxel and tariquidar overcomes tumor drug resistance. J Control Release. 2009;136(1):21-9.

68. Patil YB, Swaminathan SK, Sadhukha T, Ma L, Panyam J. The use of nanoparticle-mediated targeted gene silencing and drug delivery to overcome tumor drug resistance. Biomaterials. 2010;31(2):358-65.

69. Ganta S, Amiji M. Coadministration of Paclitaxel and curcumin in nanoemulsion formulations to overcome multidrug resistance in tumor cells. Mol Pharm. 2009;6(3):928-39.

70. Chen AM, Zhang M, Wei D, Stueber D, Taratula O, Minko T, et al. Co-delivery of doxorubicin and Bcl-2 siRNA by mesoporous silica nanoparticles enhances the efficacy of chemotherapy in multidrug-resistant cancer cells. Small. 2009;5(23):2673-7.

71. Casey JL, Coley AM, Tilley LM, Foley M. Green fluorescent antibodies: novel in vitro tools. Protein Eng. 2000;13(6):445-52.

72. Hayashi N, Kipriyanov S, Fuchs P, Welschof M, Dorsam H, Little M. A single expression system for the display, purification and conjugation of single-chain antibodies. Gene. 1995;160(1):129-30.

73. Schneider P. Production of recombinant TRAIL and TRAIL receptor: Fc chimeric proteins. Methods Enzymol. 2000;322:325-45.

74. Siemers NO, Kerr DE, Yarnold S, Stebbins MR, Vrudhula VM, Hellstrom I, et al. Construction, expression, and activities of L49-sFv-beta-lactamase, a single-chain antibody fusion protein for anticancer prodrug activation. Bioconjug Chem. 1997;8(4):510-9.

75. Knop K, Hoogenboom R, Fischer D, Schubert US. Poly(ethylene glycol) in drug delivery: pros and cons as well as potential alternatives. Angew Chem Int Ed. 2010;49(36):6288-308.

76. Alexis F, Pridgen E, Molnar LK, Farokhzad OC. Factors affecting the clearance and biodistribution of polymeric nanoparticles. Mol Pharm. 2008;5(4):505-15.

77. Morales CS, Zhang L, Langer R, Farokhzad O. Understanding the immunological properties of functionalized lipid-polymeric nanoparticles. Proceedings of the American Association for Cancer Research Annual Meeting. 2009;50:151-2.

78. Koide H, Asai T, Hatanaka K, Shimizu K, Yokoyama M, Ishida T, et al. Elucidation of Accelerated Blood Clearance Phenomenon Caused by Repeat Injection of PEGylated Nanocarriers. Yakugaku Zasshi-J Pharm Soc Jpn. 2009;129(12):1445-51.

79. Yuan F, Dellian M, Fukumura D, Leunig M, Berk DA, Torchilin VP, et al. Vascular permeability in a human tumor xenograft: molecular size dependence and cutoff size. Cancer Res. 1995;55(17):3752-6.

80. Torchilin VP. Recent advances with liposomes as pharmaceutical carriers. Nat Rev Drug Discov. 2005;4(2):145-60.

81. Hobbs SK, Monsky WL, Yuan F, Roberts WG, Griffith L, Torchilin VP, et al. Regulation of transport pathways in tumor vessels: role of tumor type and microenvironment. Proc Natl Acad Sci USA. 1998;95(8):4607-12.

82. Couvreur P, Vauthier C. Nanotechnology: intelligent design to treat complex disease. Pharm Res. 2006;23(7):1417-50.

83. Wang AZ, Gu F, Zhang L, Chan JM, Radovic-Moreno A, Shaikh MR, et al. Biofunctionalized targeted nanoparticles for therapeutic applications. Expert Opin Biol Ther. 2008;8(8):1063-70.

84. Bonadonna G, Zucali R, Monfardini S, De Lena M, Uslenghi C. Combination chemotherapy of Hodgkin's disease with adriamycin, bleomycin, vinblastine, and imidazole carboxamide versus MOPP. Cancer. 1975;36(1):252-9.

85. Scheithauer W, Rosen H, Kornek GV, Sebesta C, Depisch D. Randomised comparison of combination chemotherapy plus supportive care with supportive care alone in patients with metastatic colorectal cancer. BMJ. 1993;306(6880):752-5. PMCID: 1677246.

86. Bradshaw DM, Arceci RJ. Clinical relevance of transmembrane drug efflux as a mechanism of multidrug resistance. J Clin Oncol. 1998;16(11):3674-90.

87. Tanabe M, Ito Y, Tokudome N, Sugihara T, Miura H, Takahashi S, et al. Possible use of combination chemotherapy with mitomycin C and methotrexate for metastatic breast cancer pretreated with anthracycline and taxanes. Breast Cancer. 2009;16(4):301-6.

88. Muggia F. Platinum compounds 30 years after the introduction of cisplatin: implications for the treatment of ovarian cancer. Gynecol Oncol. 2009;112(1):275-81.

89. Berhoune M, Banu E, Scotte F, Prognon P, Oudard S, Bonan B. Therapeutic strategy for treatment of metastatic non-small cell lung cancer. Ann Pharmacother. 2008;42(11):1640-52.

90. Song XR, Cai Z, Zheng Y, He G, Cui FY, Gong DQ, et al. Reversion of multidrug resistance by co-encapsulation of vincristine and verapamil in PLGA nanoparticles. Eur J Pharm Sci. 2009;37(3-4):300-5.

91. Ahmed F, Pakunlu RI, Brannan A, Bates F, Minko T, Discher DE. Biodegradable polymersomes loaded with both paclitaxel and doxorubicin permeate and shrink tumors, inducing apoptosis in proportion to accumulated drug. J Control Release. 2006;116(2):150-8.

92. Zhang L, Radovic-Moreno AF, Alexis F, Gu FX, Basto PA, Bagalkot V, et al. Co-delivery of hydrophobic and hydrophilic drugs from nanoparticle-aptamer bioconjugates. ChemMedChem. 2007;2(9):1268-71.

93. Lammers T, Subr V, Ulbrich K, Peschke P, Huber PE, Hennink WE, et al. Simultaneous delivery of doxorubicin and gemcitabine to tumors in vivo using prototypic polymeric drug carriers. Biomaterials. 2009;30(20):3466-75.

94. Bae Y, Diezi TA, Zhao A, Kwon GS. Mixed polymeric micelles for combination cancer chemotherapy through the concurrent delivery of multiple chemotherapeutic agents. J Control Release. 2007;122(3):324-30.

95. Kolishetti N, Dhar S, Valencia PM, Lin LQ, Karnik R, Lippard SJ, et al. Engineering of self-assembled nanoparticle platform for precisely controlled combination drug therapy. Proc Natl Acad Sci USA. 2010;107:17939-44.

96. Sengupta S, Eavarone D, Capila I, Zhao G, Watson N, Kiziltepe T, et al. Temporal targeting of tumour cells and neovasculature with a nanoscale delivery system. Nature. 2005;436(7050):568-72.

97. Aryal S, Hu CM, Zhang L. Combinatorial drug conjugation enables nanoparticle dual-drug delivery. Small. 2010;6(13):1442-8.

98. Tong R, Cheng J. Controlled synthesis of camptothecin-polylactide conjugates and nanoconjugates. Bioconjug Chem. 2010;21(1):111-21.

99. Tong R, Cheng J. Paclitaxel-initiated, controlled polymerization of lactide for the formulation of polymeric nanoparticulate delivery vehicles. Angew Chem Int Ed. 2008;47(26):4830-4.

100. Tong R, Cheng J. Ring-opening polymerization-mediated controlled formulation of polylactide-drug nanoparticles. J Am Chem Soc. 2009;131(13):4744-54.

101. Chamberlain BM, Cheng M, Moore DR, Ovitt TM, Lobkovsky EB, Coates GW. Polymerization of lactide with zinc and magnesium beta-diiminate complexes: stereocontrol and mechanism. J Am Chem Soc. 2001;123(14):3229-38.

102. Chan JM, Zhang L, Yuet KP, Liao G, Rhee JW, Langer R, et al. PLGA-lecithin-PEG core-shell nanoparticles for controlled drug delivery. Biomaterials. 2009;30(8):1627-34.

103. Hu CM, Kaushal S, Tran Cao HS, Aryal S, Sartor M, Esener S, et al. Half-antibody functionalized lipid-polymer hybrid nanoparticles for targeted drug delivery to carcinoembryonic antigen presenting pancreatic cancer cells. Mol Pharm. 2010;7(3):914-20.

104. Masquelier M, Baurain R, Trouet A. Amino acid and dipeptide derivatives of daunorubicin. 1. Synthesis, physicochemical properties, and lysosomal digestion. J Med Chem. 1980;23(11):1166-70.

105. Dubowchik GM, Walker MA. Receptor-mediated and enzyme-dependent targeting of cytotoxic anticancer drugs. Pharmacol Ther. 1999;83(2):67-123.

106. Jemal A, Siegel R, Ward E, Hao Y, Xu J, Thun MJ. Cancer statistics, 2009. CA Cancer J Clin. 2009;59(4):225-49.

107. Bria E, Milella M, Gelibter A, Cuppone F, Pino MS, Ruggeri EM, et al. Gemcitabine-based combinations for inoperable pancreatic cancer: have we made real progress? A meta-analysis of 20 phase 3 trials. Cancer. 2007;110(3):525-33.

108. Olive KP, Jacobetz MA, Davidson CJ, Gopinathan A, McIntyre D, Honess D, et al. Inhibition of Hedgehog signaling enhances delivery of chemotherapy in a mouse model of pancreatic cancer. Science. 2009;324(5933):1457-61.

109. Zhang L, Chan JM, Gu FX, Rhee J-W, Wang AZ, Radovic-Moreno AF, et al. Self-assembled lipid-polymer hybrid nanoparticles: A robust drug delivery platform. ACS Nano. 2008;2(8):1696-702.

110. Ona FV, Zamcheck N, Dhar P, Moore T, Kupchik HZ. Carcinoembryonic antigen (CEA) in the diagnosis of pancreatic cancer. Cancer. 1973;31(2):324-7.

111. Kaushal S, McElroy MK, Luiken GA, Talamini MA, Moossa AR, Hoffman RM, et al. Fluorophore-conjugated anti-CEA antibody for the intraoperative imaging of pancreatic and colorectal cancer. J Gastrointest Surg. 2008;12(11):1938-50.

112. Tiefenauer LX, Kuhne G, Andres RY. Antibody-magnetite nanoparticles: in vitro characterization of a potential tumor-specific contrast agent for magnetic resonance imaging. Bioconjug Chem. 1993;4(5):347-52.

113. Maruyama K, Takahashi N, Tagawa T, Nagaike K, Iwatsuru M. Immunoliposomes bearing polyethyleneglycol-coupled Fab' fragment show prolonged circulation time and high extravasation into targeted solid tumors in vivo. FEBS Lett. 1997;413(1):177-80.

114. Pan J, Yang Q. Antibody-functionalized magnetic nanoparticles for the detection of carcinoembryonic antigen using a flow-injection electrochemical device. Anal Bioanal Chem. 2007;388(1):279-86.

115. Mastrobattista E, Koning GA, Storm G. Immunoliposomes for the targeted delivery of antitumor drugs. Adv Drug Deliv Rev. 1999;40(1-2):103-27.

116. Jackson H, Bacon L, Pedley RB, Derbyshire E, Field A, Osbourn J, et al. Antigen specificity and tumour targeting efficiency of a human carcinoembryonic antigen-specific scFv and affinity-matured derivatives. Br J Cancer. 1998;78(2):181-8. PMCID: 2062911.

117. Yazaki PJ, Shively L, Clark C, Cheung CW, Le W, Szpikowska B, et al. Mammalian expression and hollow fiber bioreactor production of recombinant anti-CEA diabody and minibody for clinical applications. J Immunol Methods. 2001;253(1-2):195-208.

118. Yazaki PJ, Wu AM, Tsai SW, Williams LE, Ikler DN, Wong JY, et al. Tumor targeting of radiometal labeled anti-CEA recombinant T84.66 diabody and t84.66 minibody: comparison to radioiodinated fragments. Bioconjug Chem. 2001;12(2):220-8.

119. Xing Y, Chaudry Q, Shen C, Kong KY, Zhau HE, Chung LW, et al. Bioconjugated quantum dots for multiplexed and quantitative immunohistochemistry. Nat Protoc. 2007;2(5):1152-65.

120. Yoon TJ, Yu KN, Kim E, Kim JS, Kim BG, Yun SH, et al. Specific targeting, cell sorting, and bioimaging with smart magnetic silica core-shell nanomaterials. Small. 2006;2(2):209-15.

121. Goldstein JL, Anderson RG, Brown MS. Coated pits, coated vesicles, and receptor-mediated endocytosis. Nature. 1979;279(5715):679-85.

122. Jiang W, Kim BY, Rutka JT, Chan WC. Nanoparticle-mediated cellular response is size-dependent. Nat Nanotechnol. 2008;3(3):145-50.

123. Kim YJ, Bang S, Park JY, Park SW, Chung JB, Song SY. Phase II study of 5-fluorouracil and paclitaxel in patients with gemcitabine-refractory pancreatic cancer. Cancer Chemo Pharma. 2009;63:529-33.

124. Moghimi SM, Hunter AC, Murray JC. Long-circulating and target-specific nanoparticles: theory to practice. Pharmacol Rev. 2001;53(2):283-318.

125. Davis ME, Chen ZG, Shin DM. Nanoparticle therapeutics: an emerging treatment modality for cancer. Nat Rev Drug Discov. 2008;7(9):771-82.

126. Peer D, Karp JM, Hong S, FaroKHzad OC, Margalit R, Langer R. Nanocarriers as an emerging platform for cancer therapy. Nat Nanotechnol. 2007;2(12):751-60.

127. Yoo JW, Chambers E, Mitragotri S. Factors that control the circulation time of nanoparticles in blood: challenges, solutions and future prospects. Curr Pharm Des. 2010;16(21):2298-307.

128. Geng Y, Dalhaimer P, Cai SS, Tsai R, Tewari M, Minko T, et al. Shape effects of filaments versus spherical particles in flow and drug delivery. Nat Nanotechnol. 2007;2(4):249-55.

129. Alexis F, Pridgen E, Molnar LK, Farokhzad OC. Factors affecting the clearance and biodistribution of polymeric nanoparticles. Mol Pharm. 2008;5(4):505-15.

130. Jiang SY, Cao ZQ. Ultralow-fouling, functionalizable, and hydrolyzable zwitterionic materials and their derivatives for biological applications. Adv Mater. 2010;22(9):920-32.

131. Yang W, Zhang L, Wang S, White AD, Jiang S. Functionalizable and ultra stable nanoparticles coated with zwitterionic poly(carboxybetaine) in undiluted blood serum. Biomaterials. 2009;30(29):5617-21.

132. Doshi N, Zahr AS, Bhaskar S, Lahann J, Mitragotri S. Red blood cell-mimicking synthetic biomaterial particles. Proc Natl Acad Sci USA. 2009;106(51):21495-9.

133. Tsai RK, Rodriguez PL, Discher DE. Self inhibition of phagocytosis: the affinity of 'marker of self' CD47 for SIRPalpha dictates potency of inhibition but only at low expression levels. Blood Cells Mol Dis. 2010;45(1):67-74. PMCID: 2878922.

134. Merkel TJ, Jones SW, Herlihy KP, Kersey FR, Shields AR, Napier M, et al. Using mechanobiological mimicry of red blood cells to extend circulation times of hydrogel microparticles. Proc Natl Acad Sci U S A. 2011;108(2):586-91.

135. Dodge JT, Mitchell C, Hanahan DJ. The preparation and chemical characteristics of hemoglobin-free ghosts of human erythrocytes. Arch Biochem Biophys. 1963;100:119-30.

136. Waugh RE, Sarelius IH. Effects of lost surface area on red blood cells and red blood cell survival in mice. Am J Physiol. 1996;271(6 Pt 1):C1847-52.

137. Arnold MM, Gorman EM, Schieber LJ, Munson EJ, Berkland C. NanoCipro encapsulation in monodisperse large porous PLGA microparticles. J Control Release. 2007;121(1-2):100-9. PMCID: 2041842.

138. Jacobs RL, Alling DW, Cantrell WF. An evaluation of antimalarial combinations against plasmodium berghei in the mouse. J Parasitol. 1963;49:920-5.

139. Desilets J, Lejeune A, Mercer J, Gicquaud C. Nanoerythrosomes, a new derivative of erythrocyte ghost: IV. Fate of reinjected nanoerythrosomes. Anticancer Res. 2001;21(3B):1741-7.

140. Cheng J, Teply BA, Sherifi I, Sung J, Luther G, Gu FX, et al. Formulation of functionalized PLGA-PEG nanoparticles for in vivo targeted drug delivery. Biomaterials. 2007;28(5):869-76.

141. Tanaka M, Sackmann E. Polymer-supported membranes as models of the cell surface. Nature. 2005;437(7059):656-63.

142. Hochmuth RM, Evans CA, Wiles HC, McCown JT. Mechanical measurement of red cell membrane thickness. Science. 1983;220(4592):101-2.

143. Fang RH, Aryal S, Hu CM, Zhang L. Quick synthesis of lipid-polymer hybrid nanoparticles with low polydispersity using a single-step sonication method. Langmuir. 2010;26:16958-62.

144. Popielarski SR, Pun SH, Davis ME. A nanoparticle-based model delivery system to guide the rational design of gene delivery to the liver. 1. Synthesis and characterization. Bioconjug Chem. 2005;16(5):1063-70.

145. Goutayer M, Dufort S, Josserand V, Royere A, Heinrich E, Vinet F, et al. Tumor targeting of functionalized lipid nanoparticles: assessment by in vivo fluorescence imaging. Eur J Pharm Biopharm. 2010;75(2):137-47.

146. Xiao K, Luo J, Fowler WL, Li Y, Lee JS, Xing L, et al. A self-assembling nanoparticle for paclitaxel delivery in ovarian cancer. Biomaterials. 2009;30(30):6006-16. PMCID: 2735593.

147. Gratton SE, Pohlhaus PD, Lee J, Guo J, Cho MJ, Desimone JM. Nanofabricated particles for engineered drug therapies: a preliminary biodistribution study of PRINT nanoparticles. J Control Release. 2007;121(1-2):10-8.

148. Peracchia MT, Fattal E, Desmaele D, Besnard M, Noel JP, Gomis JM, et al. Stealth PEGylated polycyanoacrylate nanoparticles for intravenous administration and splenic targeting. J Control Release. 1999;60(1):121-8.

149. Simberg D, Duza T, Park JH, Essler M, Pilch J, Zhang L, et al. Biomimetic amplification of nanoparticle homing to tumors. Proc Natl Acad Sci U S A. 2007;104(3):932-6.

150. Oldenborg PA, Zheleznyak A, Fang YF, Lagenaur CF, Gresham HD, Lindberg FP. Role of CD47 as a marker of self on red blood cells. Science. 2000;288(5473):2051-4.

151. Gu F, Zhang L, Teply BA, Mann N, Wang A, Radovic-Moreno AF, et al. Precise engineering of targeted nanoparticles by using self-assembled biointegrated block copolymers. Proc Natl Acad Sci USA. 2008;105(7):2586-91. PMCID: 2268180.

152. Avgoustakis K, Beletsi A, Panagi Z, Klepetsanis P, Livaniou E, Evangelatos G, et al. Effect of copolymer composition on the physicochemical characteristics, in vitro stability, and biodistribution of PLGA-mPEG nanoparticles. Int J Pharm. 2003;259(1-2):115-27.

153. Zhang L, Zhang L. Lipid-polymer hybrid nanoparticles: synthesis, characterization and applications. Nano LIFE. 2010;1(1&2):163-73.

154. Sengupta S, Eavarone D, Capila I, Zhao G, Watson N, Kiziltepe T, et al. Temporal targeting of tumour cells and neovasculature with a nanoscale delivery system. Nature. 2005;436:568-72.

155. Valencia PM, Basto PA, Zhang L, Rhee M, Langer R, Farokhzad OC, et al. Single-step assembly of homogenous lipid-polymeric and lipid-quantum dot nanoparticles enabled by microfluidic rapid mixing. ACS Nano. 2010;4(3):1671-9. PMCID: 2923464.

156. Liu J, Stace-Naughton A, Jiang X, Brinker CJ. Porous nanoparticle supported lipid bilayers (protocells) as delivery vehicles. J Am Chem Soc. 2009;131(4):1354-5. PMCID: 2649781.

157. van Schooneveld MM, Gloter A, Stephan O, Zagonel LF, Koole R, Meijerink A, et al. Imaging and quantifying the morphology of an organic-inorganic nanoparticle at the sub-nanometre level. Nat Nanotechnol. 2010;5(7):538-44.